

# Hanford Tank Farms Vadose Zone Monitoring Project

## 2002 Recalibration of the Radionuclide Logging System

Carl J. Koizumi

March 2004



U.S. Department  
of Energy



This report was prepared as an account of work sponsored by an agency of the United States Government. Neither the United States Government nor any agency thereof, nor any of their employees, makes any warranty, express or implied, or assumes any legal liability or responsibility for the accuracy, completeness, or usefulness of any information, apparatus, product, or process disclosed in this report, or represents that its use would not infringe privately owned rights. Reference herein to any specific commercial product, process, or service by trade name, trademark, manufacturer, or otherwise, does not necessarily constitute or imply its endorsement, recommendation, or favoring by the United States Government or any agency thereof. The views and opinions of authors expressed herein do not necessarily state or reflect those of the United States Government or any agency thereof.

**Hanford Tank Farms Vadose Zone Monitoring Project**

**2002 Recalibration of the  
Radionuclide Logging System**

**March 2004**

Prepared for  
U.S. Department of Energy  
Office of Environmental Management  
Grand Junction, Colorado

Prepared by  
S.M. Stoller Corp.  
Grand Junction, Colorado

Approved for public release; distribution is unlimited.  
Work performed under DOE Contract No. DE-AC01-02GJ79491.

# Contents

	Page
Signature Page.....	vi
<b>1.0 Introduction</b> .....	<b>1</b>
<b>2.0 Radionuclide Assessment System</b> .....	<b>2</b>
<b>3.0 System Measurement Effects</b> .....	<b>5</b>
3.1 Dead Time Effect .....	5
3.2 Pre-Deployment Gain Stability Tests.....	5
3.3 2002 System Stability Tests .....	5
3.3.1 Large Detector Test .....	5
3.3.1.1 Addendum to the Large Detector Stability Test.....	14
3.3.2 Small Detector Stability Tests .....	17
3.3.3 Medium Detector Stability Tests .....	20
3.3.4 Recommendations.....	25
<b>4.0 Calibration Measurements</b> .....	<b>27</b>
4.1 Data Acquisition.....	27
4.2 Use of Calibration Data.....	30
<b>5.0 Revised Field Verification Acceptance Criteria</b> .....	<b>32</b>

## List of Tables

Table 2-1. Features of the Three RAS NaI(Tl) Detectors .....	2
2-2. RAS Window Settings .....	3
3-1. Position of the 1764.5-keV Gamma-Ray Peak during the Small Detector Stability Test.....	19
3-2. Position of the 1764.5-keV Gamma-Ray Peak during the Medium Detector Stability Test.....	21
4-1. Calibration Measurement Details .....	27
4-2. Calibration Count Rate Data for the Small Detector .....	28
4-3. Calibration Count Rate Data for the Medium Detector .....	28
4-4. Calibration Count Rate Data for the Large Detector .....	28
4-5. Small Detector 2002 Count Rate Data (no sleeve).....	29
4-6. Small Detector 2000 Count Rate Data (no sleeve).....	29
4-7. Medium Detector 2002 Count Rate Data .....	29
4-8. Medium Detector 2000 Count Rate Data (no sleeve) .....	29
4-9. Large Detector 2002 Calibration Count Rate Data .....	29
4-10. Large Detector 2000 Calibration Count Rate Data.....	30
5-1. Sources in the KUTH Field Verifier.....	32

## Contents (continued)

	Page
Table 5-2. Large Detector Field Verification Data .....	33
5-3. Large Detector Control Limits .....	33
5-4. Medium Detector Field Verification Data .....	33
5-5. Medium Detector Control Limits .....	34
5-6. Small Detector Field Verification Data .....	34
5-7. Small Detector Control Limits .....	34

### List of Figures

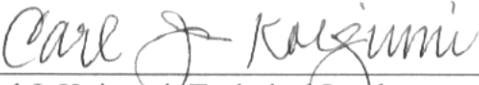
Figure 3-1. Two Pulse Height Spectra Recorded for a Stability Test with the RAS Large Detector .....	6
3-2. Total Count Rate Plotted in Relation to Spectrum Number .....	7
3-3. Ratio of Count Rate to Average Count Rate Plotted in Relation to Spectrum Number .....	8
3-4. Lithology Window Stability Data .....	9
3-5. Cesium, Mid-Range, and Protactinium Window Stability Data .....	10
3-6. Cobalt, Potassium, Uranium, and Thorium Window Stability Data .....	10
3-7. Large Detector Gain Shift Illustration .....	11
3-8. Stability of Lithology Window Count Rates when Window Settings are Adjusted for Gain Shift .....	12
3-9. Stability of Cesium, Mid-Range, and Protactinium Window Count Rates when Window Settings are Adjusted for Gain Shift .....	13
3-10. Stability of Cobalt, Potassium, and Uranium Window Count Rates when Window Settings are Adjusted for Gain Shift .....	13
3-11. Stability of Thorium Window Count Rates when Window Settings are Adjusted for Gain Shift .....	14
3-12. Stability Test after Power Supply Replacement .....	15
3-13. Comparison of Efficiency Changes over Time .....	16
3-14. Relative Efficiency Changes over Time .....	16
3-15. Relative Changes in Count Rate over Time .....	17
3-16. First Small Detector Gain Stability Test .....	18
3-17. Second Small Detector Gain Stability Test .....	18
3-18. Gain Shift during Small Detector Stability Test .....	19
3-19. Relative Change in Efficiency during Small Detector Stability Test .....	20
3-20. Gain Shift during Medium Detector Stability Test .....	21
3-21. Relative Change in Efficiency during Medium Detector Stability Test .....	22
3-22. Relative Change in Lithology Window Count Rate during Medium Detector Stability Test .....	23
3-23. Relative Changes in Cesium and Cobalt Window Count Rates during Medium Detector Stability Test .....	24

## Contents (continued)

	<b>Page</b>
Figure 3-24. Relative Changes in Thorium Window Count Rates during Medium Detector Stability Test.....	25
<b>List of References</b> .....	<b>35</b>
<b>Appendix A. Gamma-Ray Calibration Standards</b> .....	<b>A-1</b>

**Hanford Tank Farms Vadose Zone Monitoring Project  
2002 Recalibration of the Radionuclide Assessment System**

**Prepared by:**

  
\_\_\_\_\_  
Carl J. Koizumi, Technical Lead  
S.M. Stoller, Grand Junction, CO

03-30-2004  
Date

**Concurrence:**

  
\_\_\_\_\_  
R.G. McCain, Hanford Technical Lead  
S.M. Stoller, Hanford, Richland, WA

04-07-2004  
Date

**Approved by:**

  
\_\_\_\_\_  
Brian Mathis, Project Manager  
S.M. Stoller, Hanford, Richland, WA

04/07/04  
Date

# 1.0 Introduction

During 1995-2000, the U.S. Department of Energy (DOE) Grand Junction Site logged approximately 760 boreholes in the DOE Hanford Site tank farms with high-purity germanium (HPGe) sensors. Using full-energy peaks in the high-resolution spectra, gamma-ray-emitting radionuclides were identified and the in situ concentrations were determined, usually with accuracies comparable to laboratory sample assays.

Radionuclides of interest included fission fragments, neutron activation products, and processed uranium. Wastes containing these radionuclides are byproducts of decades of operations at the Hanford Site that produced plutonium for the national defense. The wastes were introduced to the subsurface by leaks in buried waste storage tanks, surface spills, and other inadvertent releases in the tank farms.

Geostatistical analyses of radionuclide concentration data produced three-dimensional depictions of waste plumes in the subsurface. Reports that present these results, along with other findings, are posted at the Internet address <http://www.gjo.doe.gov/programs/hanf/HTFVZ.html>.

Because logging acquires in situ data without disturbing the material being sampled, log measurements can be repeated at intervals to interrogate for changes. Contaminated subsurface zones in the Hanford tank farms are now being periodically re-logged to monitor for evidence of contaminant migration. The monitoring system, named the Radionuclide Assessment System (RAS), is less complicated than the HPGe-based systems and acquires data using faster logging speeds and simpler operations. The RAS is equipped with three thallium-activated sodium iodide (NaI(Tl)) detectors. Low-resolution spectra acquired with these detectors are suitable for detection of changes in the subsurface radiation intensities, but concentrations of gamma-ray-emitting radionuclides can be estimated only under certain extremely favorable circumstances.

“Calibration” of the RAS is the subject of this report. Because radionuclide concentrations are not objectives, the RAS is not calibrated in the usual sense. That is, correlations between instrument responses and concentrations have not been derived. Instead, certain characteristics of the system have been determined, and are described in this report.

During logging operations, a portable, sealed potassium-uranium-thorium source is periodically used to record data to verify the performance of the logging system. A performance test is conducted by recording a spectrum, calculating count rates in specific portions of the spectrum and comparing the rates to acceptance tolerances, or “field verification criteria.” The field verification criteria are revised at each recalibration. This report presents revised criteria that were derived from 12 spectra that were recorded during the acquisition of calibration data.

## 2.0 Radionuclide Assessment System

The RAS is a mobile, self-contained logging system that acquires low-resolution passive gamma-ray spectra. The sonde has an upper section containing a multichannel analyzer and the telemetry components. Any one of three modules can be connected to this section. Each module has a NaI(Tl) crystal and photomultiplier. Table 2-1 shows dimensions and other features of the three detector crystals.

Table 2-1. Features of the Three RAS NaI(Tl) Detectors

Informal Name	Crystal Diameter and Length (inches)	Intended Use
Small detector	1.0 by 1.0	This low-efficiency detector is designed to acquire passive gamma-ray spectra in intense radiation fields. Radiation is collimated by 1-inch-thick lead shields above and below the crystal.
Medium detector	1.5 by 2.0	This medium-efficiency detector is designed to acquire passive gamma-ray spectra in moderate radiation fields. There is no lead shielding around this crystal.
Large detector	3.0 by 12.0	This high-efficiency detector is designed to acquire passive gamma-ray spectra in low radiation fields. There is no lead shielding around this crystal.

Pulse heights of pulses from any of the three detectors are determined by an analog-to-digital converter, and counts are tallied by a 256-channel multichannel analyzer (MCA). The MCA channel that registers a particular count is determined by the pulse height and the system gain, which relates pulse height to MCA channel number.

RAS spectra can be analyzed by total counts and window<sup>1</sup> counts. There are eight spectral windows for window count analysis. Settings for these windows are displayed in Table 2-2. The energy ranges were determined through reviews of window settings established for measurements supporting the 1974-1984 National Uranium Resource Evaluation (NURE<sup>2</sup>) program (Wilson and Stromswold 1981), and through analyses of spectra acquired during performance testing of the RAS at the DOE Grand Junction Site in 1996. The corresponding MCA channel number settings were determined from spectra collected in 2001 using an Amersham K-U-Th field verification source (Amersham part name: *KUTh Field Verifier*; part number: 188074).

<sup>1</sup> A window is a section of a spectrum defined by a contiguous group of MCA channels. Although the lower and upper window boundaries are set by MCA channel numbers, the two levels are usually specified in kilo-electron-volts.

<sup>2</sup> NURE was conducted by the DOE Grand Junction Site from 1974 to 1984 to assess the uranium resources of the United States. The program supported significant research and development in nuclear logging. The borehole calibration standards that are now used to calibrate radiation sensors for environmental surveys were designed and constructed under the NURE program.

Table 2-2. RAS Window Settings

Name of Window	Range (keV)	Approximate Range (MCA channel numbers)			Source and Energy of Target Gamma Ray
		Small Detector	Medium Detector	Large Detector	
Lithology <sup>1</sup>	0 – 570	0 – 52	0 – 49	0 – 52	None
Cesium-137	570 – 740	53 – 67	50 – 64	53 – 68	<sup>137</sup> Cs (661.6 keV)
Mid-Range <sup>2</sup>	740 – 940	68 – 84	65 – 80	69 – 86	None
Protactinium-234	940 – 1060	85 – 95	81 – 90	87 – 97	<sup>234m</sup> Pa <sup>3</sup> (1001.0 keV)
Cobalt-60	1060 – 1390	96 – 123	91 – 118	98 – 126	<sup>60</sup> Co (1173.2 keV, 1332.5 keV)
Potassium-40	1390 – 1600	124 – 140	119 – 135	127 – 145	<sup>40</sup> K (1460.8 keV)
Uranium-238	1600 – 2400	141 – 206	136 – 200	146 – 214	<sup>214</sup> Bi <sup>4</sup> (1764.5 keV, 2204.1 keV)
Thorium-232	2400 – 2800	207 – 255	201 – 255	215 – 255	<sup>208</sup> Tl <sup>5</sup> (2614.5 keV)

<sup>1</sup>The counts in this window will be influenced by the “Z effect.” See Section 3.1, “Dead Time Effect.”

<sup>2</sup>This window occupies the gap between the cesium-137 and protactinium-234 windows. It has no use at present.

<sup>3</sup>Protactinium-234m (<sup>234m</sup>Pa) is the third nuclide in the <sup>238</sup>U decay chain. <sup>234m</sup>Pa and the nuclide that precedes it in the decay chain, <sup>234</sup>Th, have such short half lives (1.2 minutes and 24 days) that the existence of <sup>234m</sup>Pa essentially guarantees that <sup>238</sup>U is also present. The spectral peak for the <sup>234m</sup>Pa gamma ray is rarely observed in association with natural uranium because the gamma-ray yield is so low, but a high concentration of processed <sup>238</sup>U will be revealed by a prominent peak due to the 1001.0-keV <sup>234m</sup>Pa gamma ray.

<sup>4</sup>Bismuth-214 is the tenth nuclide in the <sup>238</sup>U decay chain. Because a long-lived nuclide (radium-226, half life = 1600 years) and an inert gas (radon-222) occur between <sup>238</sup>U and <sup>214</sup>Bi in the decay chain, the existence of <sup>214</sup>Bi does not necessarily imply that <sup>238</sup>U is also present. Nonetheless, the 609.3, 1764.5, and 2204.1-keV <sup>214</sup>Bi gamma rays have high yields and are often used to assay naturally occurring <sup>238</sup>U.

<sup>5</sup>Thallium-208 is the tenth nuclide in the thorium decay chain.

Each window is set to tally counts due to gamma rays listed in the “Source and Energy of Target Gamma Ray” column of Table 2-2.

Windows are designated for the <sup>137</sup>Cs and <sup>60</sup>Co gamma rays because these two nuclides are by far the most widespread reactor-generated radionuclides detected by the high-resolution surveys.

Processed uranium (mixture of <sup>235</sup>U and <sup>238</sup>U) was also detected fairly frequently. The protactinium-234 window tallies counts associated with the 1001.0-keV <sup>234m</sup>Pa gamma ray.

The <sup>40</sup>K, <sup>238</sup>U, and <sup>232</sup>Th windows acquire counts due to prominent gamma rays from naturally occurring potassium, uranium, and thorium.

The counts acquired in a particular window usually cannot be directly correlated to the concentration of the associated gamma-ray source because windows generally contain additional counts due to gamma rays with energies higher than the window boundaries. For example, gamma rays with energies higher than 740 keV will produce background counts in the <sup>137</sup>Cs window via Compton downscattering within the detector. In particular, gamma rays from natural potassium, uranium, and thorium, and <sup>60</sup>Co will contribute to background in the <sup>137</sup>Cs window.

Other reactor-generated nuclides in Hanford waste, such as  $^{152}\text{Eu}$  and  $^{154}\text{Eu}$ , are sources of gamma rays with energies high enough to introduce backgrounds in the  $^{137}\text{Cs}$  and  $^{60}\text{Co}$  windows. In general, when the most common Hanford waste constituents are present, the  $^{137}\text{Cs}$  and  $^{60}\text{Co}$  windows will have elevated count rates, even if  $^{137}\text{Cs}$  and  $^{60}\text{Co}$  are not present. The  $^{137}\text{Cs}$  and  $^{60}\text{Co}$  window count rates therefore serve as indexes for the reactor-generated wastes. Elevated window count rates indicate the presence of waste, and changes in those count rates over time imply that the concentrations of waste constituents are changing. It is not necessary to identify the source radionuclides to infer changes in concentrations.

The naturally occurring gamma-ray sources will contribute counts to the  $^{137}\text{Cs}$  and  $^{60}\text{Co}$  windows, but the concentrations of these sources in the subsurface are expected to be constant over time. Thus, the natural emitters won't influence the monitoring for changes in the  $^{137}\text{Cs}$  and  $^{60}\text{Co}$  window count rates.

## **3.0 System Measurement Effects**

### **3.1 Dead Time Effect**

Before the RAS was deployed at Hanford, calibration standards at the Grand Junction Site with extreme concentrations of uranium (up to 7,459 pCi/g) were logged to assess system dead time effects. Evaluations of these data indicated that the dead time effect on measurements was negligible for dead times up to 35 percent for the small detector, 63 percent for the medium detector, and 69 percent for the large detector (Koizumi 2001).

The recorded total count rates were found to be linear in relation to uranium concentration for the lower concentrations, but nonlinear for the higher uranium concentrations. For the high uranium concentrations, the total count rates were lower than would be predicted using the nearly linear relationship between total count rate and uranium concentration that characterized the low uranium concentration data. Koizumi (2001) showed that this nonlinearity is a manifestation of the *Z* effect, not dead time. (*Z*, the average atomic number of the logged medium, is directly related to the uranium concentration.) Although the *Z* effect influenced the dead time measurements, it will probably affect few, if any, RAS measurements at Hanford. The *Z* effect is a consequence of photoelectric absorption, which primarily affects low energy gamma rays. The <sup>137</sup>Cs window, and the windows at higher energies, record counts from gamma rays with energies high enough to be essentially unaffected by the *Z* effect. In addition, subsurface zones at Hanford will not have anomalously high values of *Z* unless they are heavily contaminated with processed uranium or other high-*Z* contaminants.

### **3.2 Pre-deployment Gain Stability Tests**

Experiments to assess the RAS gain stability were performed before the RAS was deployed at Hanford, and are described by Koizumi (2001). Minor gain shifts accompanied temperature changes, as expected, but large gain offsets occurred when the sonde was inserted into or withdrawn from the steel casing in the test apparatus. This implied that magnetic field variations on the photomultiplier were a major cause of abrupt gain shifts. Additional support for this conjecture came from field observations in which the gain was significantly perturbed whenever the sonde encountered a weld in steel casing.

To mitigate magnetic effects, mu-metal shields were installed on the photomultiplier tubes of the small and medium detectors. The spacing around the large detector photomultiplier tube was too small to accommodate shielding.

### **3.3 2002 System Stability Tests**

#### **3.3.1 Large Detector Test**

For the large detector stability test, the sonde was placed in the SBA calibration standard (described in Appendix A) such that the detector was at the (vertical) center of the standard. There was no casing in the test hole. Next, 401 spectra were recorded, with a 30-second

acquisition time per spectrum, without moving or otherwise disturbing the sonde. The data were recorded on March 6, 2002. Data acquisition began at about 11:32 AM, and ended at about 4:32 PM.

The test yielded an example of gradual gain shifts that occur for unknown reasons. The large detector photomultiplier does not have a mu-metal shield; however, except for the conductors in the logging cable and the sonde itself, there was no metal in the calibration standard test hole. Presumably, there were no changes in the distribution of magnetic material near the sonde, and no other factors that could have affected the gain by producing large magnetic field disturbances near the photomultiplier.

The gain drifted upward during the entire 5-hour duration of the stability test. The drift rate was highest at the beginning of the test, and the rate moderated over time. Figure 3-1 depicts the first and last spectra that were recorded.

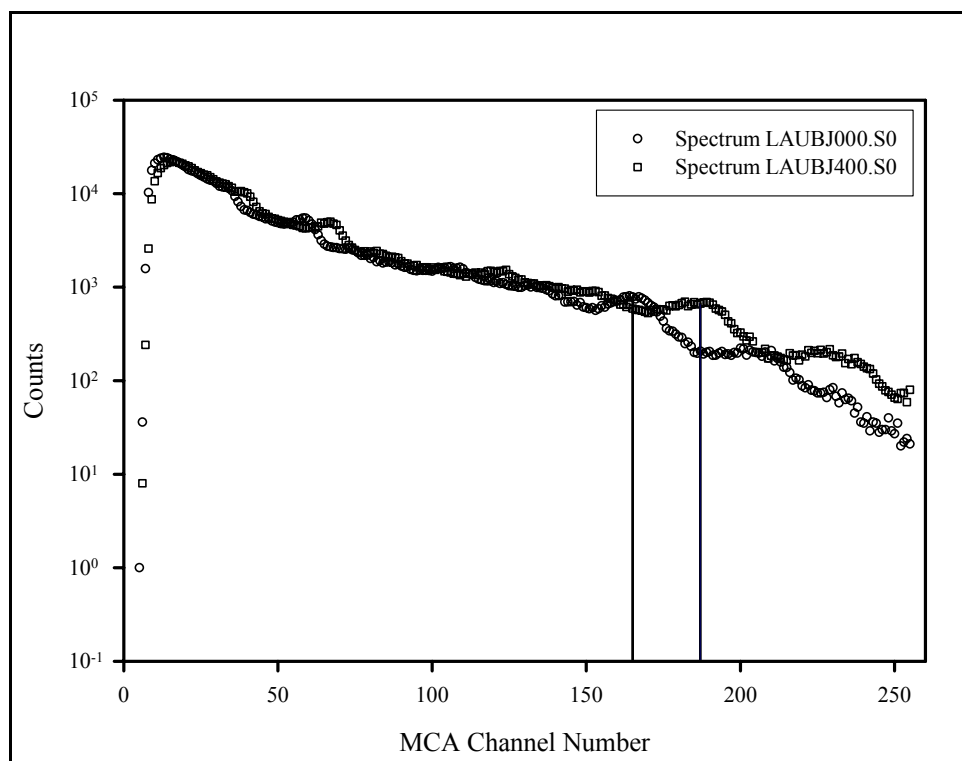


Figure 3-1. Two Pulse Height Spectra Recorded for a Stability Test with the RAS Large Detector

The first spectrum file in the series was LAUBJ000.CHN<sup>3</sup>, and LAUBJ400.CHN was the last file. The center of the full energy peak for the 1764.5-keV “uranium” gamma ray was close to MCA channel 165 in the first spectrum, and by the end of the test, the gain shift had displaced the center of the peak to a point near channel 187. The two peak centers are marked in Figure 3-1 by vertical lines. The change in position of the peak corresponded to a shift on the energy scale of about 250 keV.

<sup>3</sup> The logging unit records spectra in the Ortec format, indicated by a “CHN” file extension. Prior to analysis, the files are converted to Aptec format, indicated by an “S0” file extension.

The gain shift was accompanied by an upward drift in system efficiency. This drift is revealed by the plot of total count rate in relation to spectrum number shown in Figure 3-2. Because the spectra were collected at 30-second intervals, spectrum number is correlated to time.

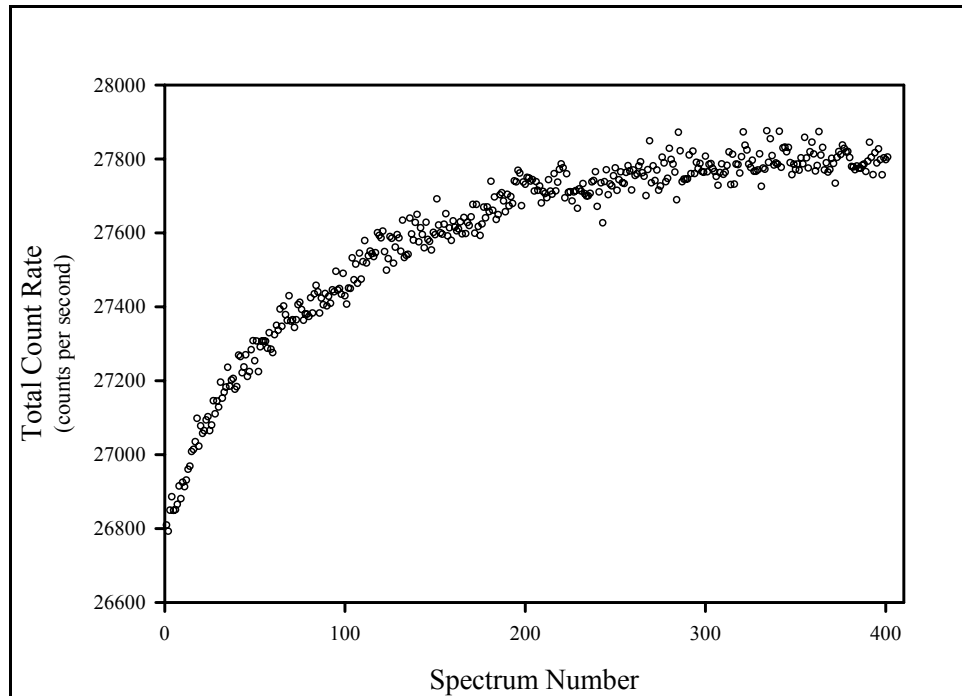


Figure 3-2. Total Count Rate Plotted in Relation to Spectrum Number

The rate of change of efficiency was high at the beginning of the test, but the graph in Figure 3-2 indicates that the rate of change moderated as the test proceeded, and the efficiency apparently reached a stable condition when the test was about 75 percent done. A minor contributor to the decrease in the rate of change of total count rate was losses of counts from the high-energy end of the spectrum caused by the upward drift in gain. When gain shift caused the pulse heights for the largest detector output pulses to exceed the value corresponding to the highest MCA channel, the corresponding counts were lost.

The fractional change, or percentage of change, is more evident if the total count rate is replaced with the ratio of the total count rate to the total count rate average. The plot in Figure 3-3 shows this ratio plotted in relation to spectrum number. The increase in count rate was a bit less than 4 percent, relative to the average count rate.

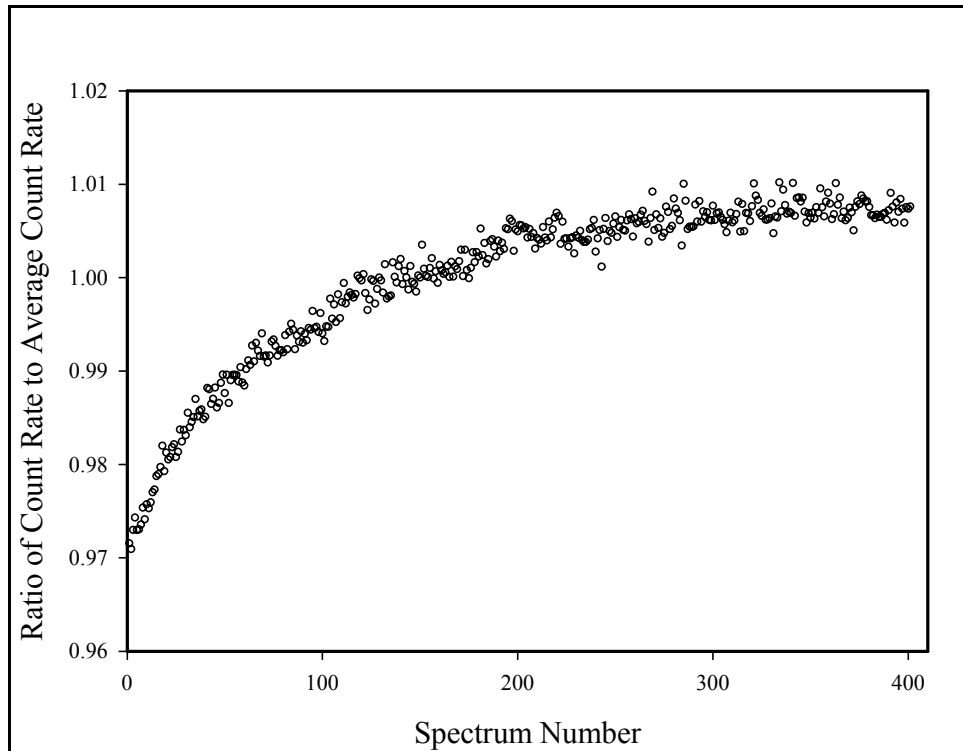


Figure 3-3. Ratio of Count Rate to Average Count Rate Plotted in Relation to Spectrum Number

The effects of gain and efficiency shifts on total counts are straightforward to measure, but the effects on window counts depend on the method of setting the spectral windows. For field data, window settings are customarily established as follows. A field verification spectrum is acquired and energy-calibrated with Aptec Engineering's *PCMCA/WIN* spectrum analysis algorithm. This energy calibration is used to establish the MCA channel numbers corresponding to the boundaries of the eight spectral windows (Table 2-2). A large set of spectra can then be batch-processed by Aptec Engineering's *Supervisor* algorithm, which can be programmed to "import" the window settings to each spectrum, then calculate the counts in each window by summing the counts in the channels within the window. By this method, many spectra can be rapidly analyzed. However, the same window settings, specified in MCA channel numbers, will be imposed on every spectrum, and effects due to gain shift may be large and susceptible to misinterpretation.

The 401 spectra from the stability test were processed using the method based on Aptec *Supervisor*. Each black circle in the plot in Figure 3-4 represents the ratio of lithology window count rate for a spectrum to average lithology window count rate for all spectra. The ratio of total count rate to average total count rate is also shown, for comparison. The lithology window data would suggest that the count rate in the lithology window decreased as the test progressed.

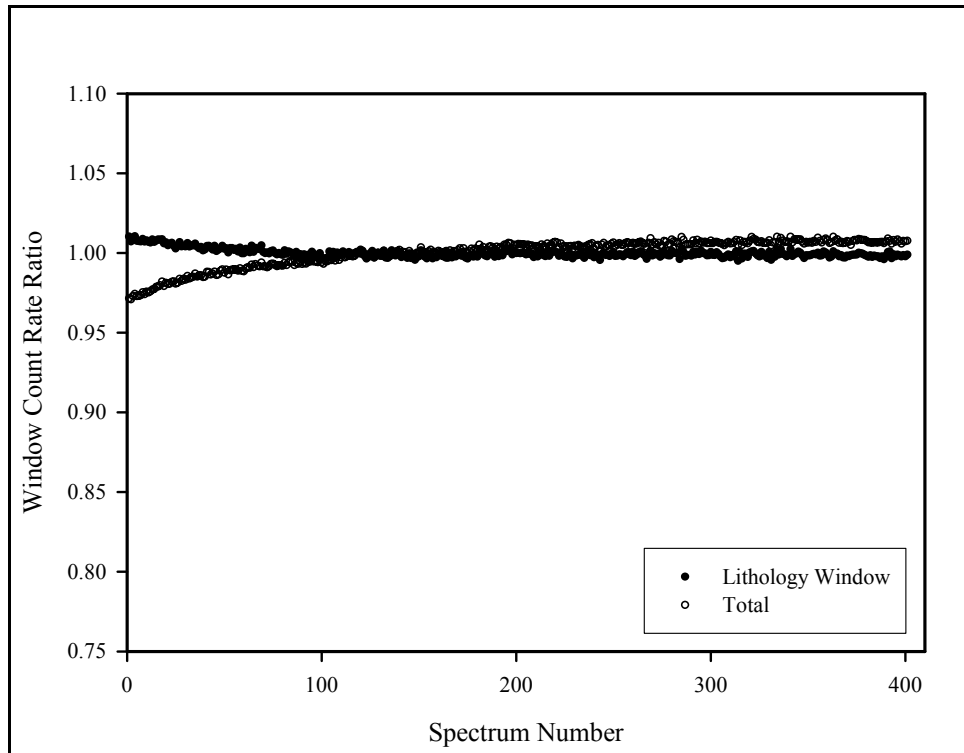


Figure 3-4. Lithology Window Stability Data

Count rates for the other windows rose as the test progressed. The trends are indicated by the plots in Figures 3-5 and 3-6. The scales on the vertical axes in Figures 3-4, 3-5, and 3-6 are identical to assist comparisons.

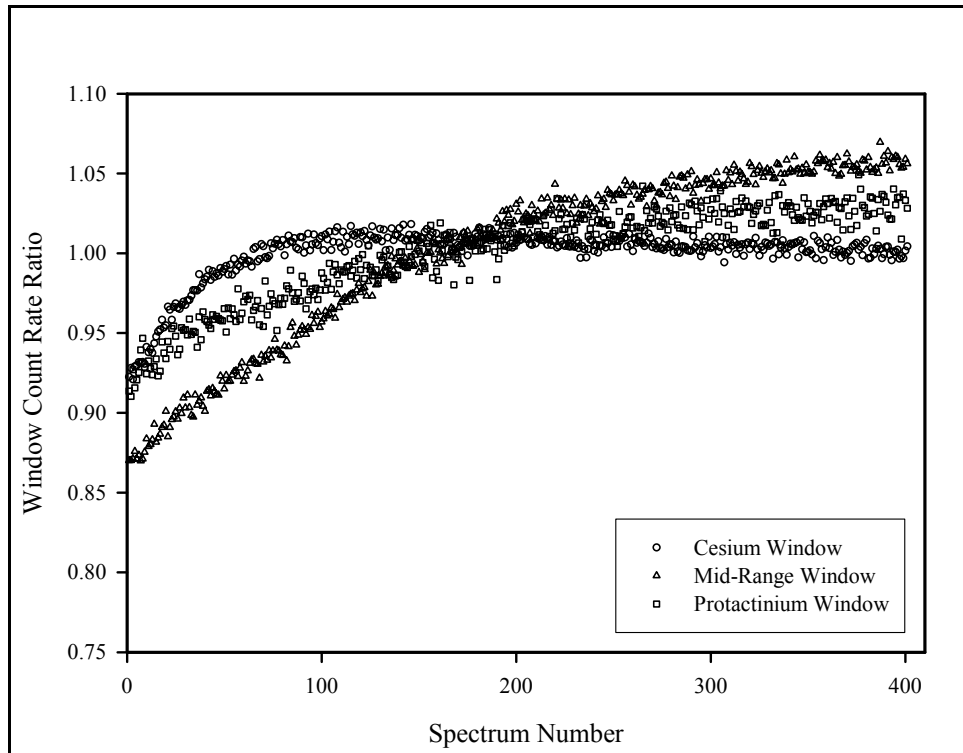


Figure 3-5. Cesium, Mid-Range, and Protactinium Window Stability Data

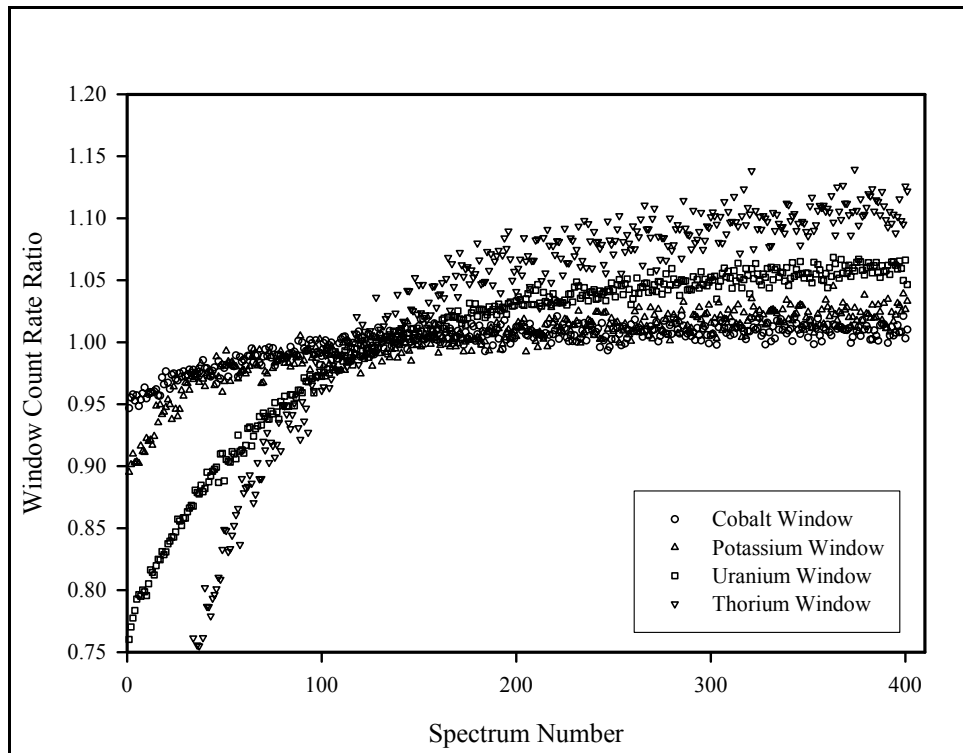


Figure 3-6. Cobalt, Potassium, Uranium, and Thorium Window Stability Data

The trends illustrated in Figures 3-4, 3-5, and 3-6 are actually artifacts of the fixed spectral window boundaries. The plots in Figure 3-7 depict the first, middle, and last spectra in the test,

and the vertical lines represent the boundaries of the spectral windows, set according to the energy calibration of the first spectrum.

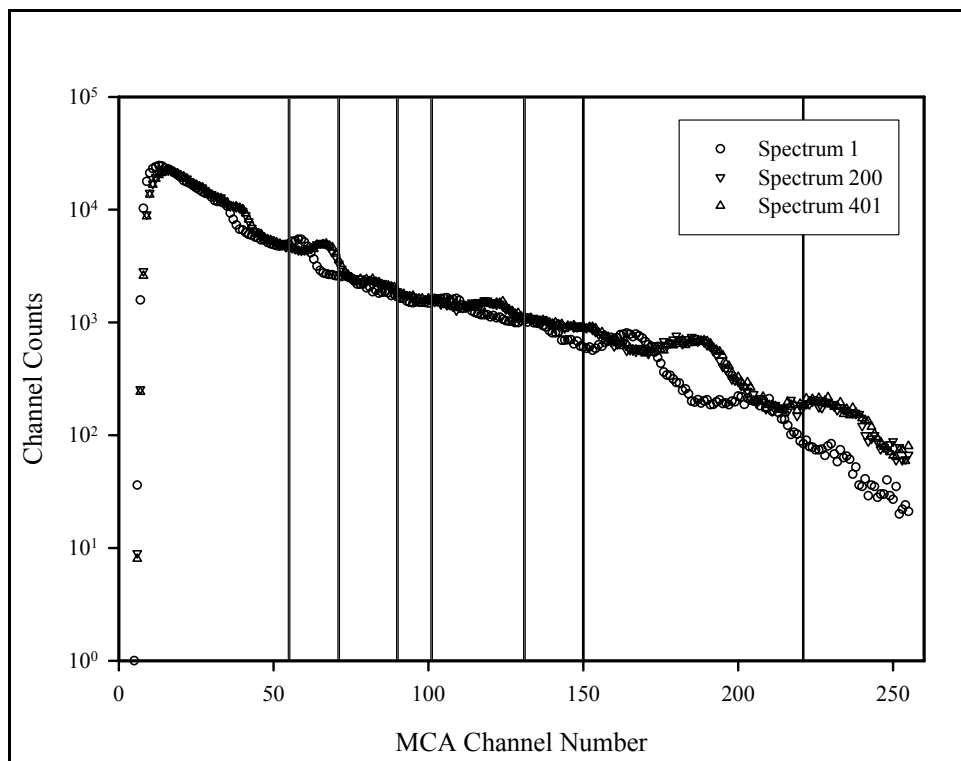


Figure 3-7. Large Detector Gain Shift Illustration

The spectra and windows in Figure 3-7 make it evident that as the gain drifts upward, the spectra “stretch” toward the right, and the number of counts in the lithology window (channels 1 through 55) should shrink, while the numbers of counts in the other windows should grow. These trends are actually observed, as indicated in Figures 3-4 through 3-6.

However, quite different trends are observed if the window boundaries are set on each spectrum according to individual spectrum energy calibrations, i.e., if the window boundaries shift along with the gain.

The even-numbered spectra were individually energy-calibrated, the window boundaries were set according to energy, and the window count rates were calculated. Figure 3-8 shows how the lithology window count rate ratio and the total count rate ratio behaved as the stability test progressed. The lithology window count rate increased in step with the total count rate. This was expected because the lithology window captures most of the counts in a spectrum, so the upward drift of system efficiency drove the lithology window count and the total window count upward.

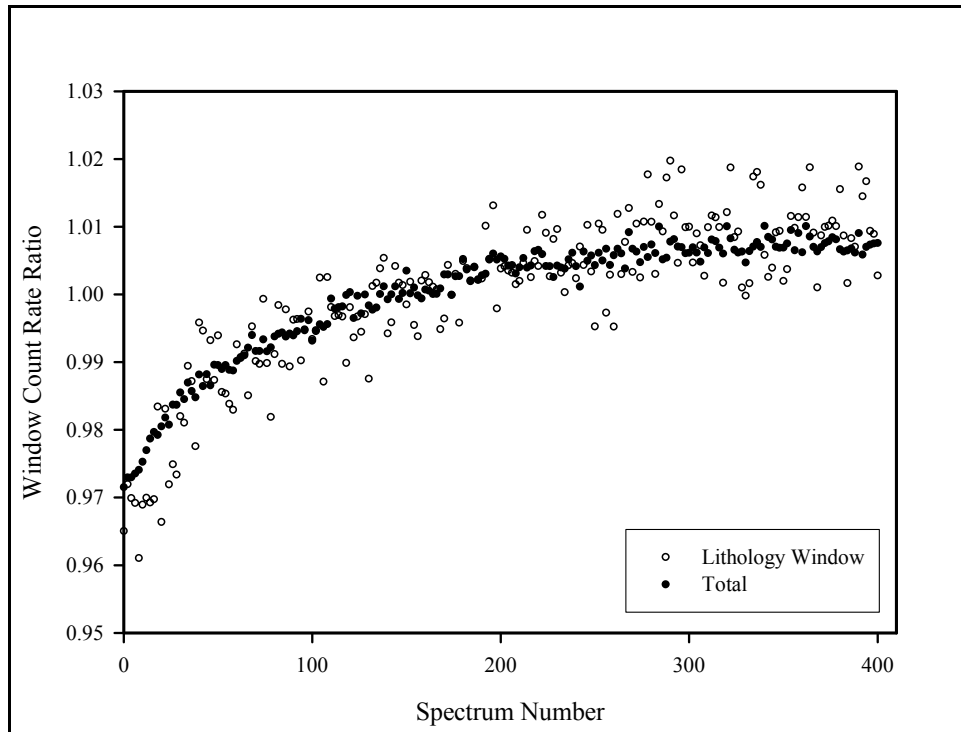


Figure 3-8. Stability of Lithology Window Count Rates when Window Settings are Adjusted for Gain Shift

For the cesium, mid-range, protactinium, cobalt, potassium, and uranium windows, the count rates did not follow discernible trends. The count rate ratios for these windows are plotted in relation to spectrum number in Figures 3-9 and 3-10.

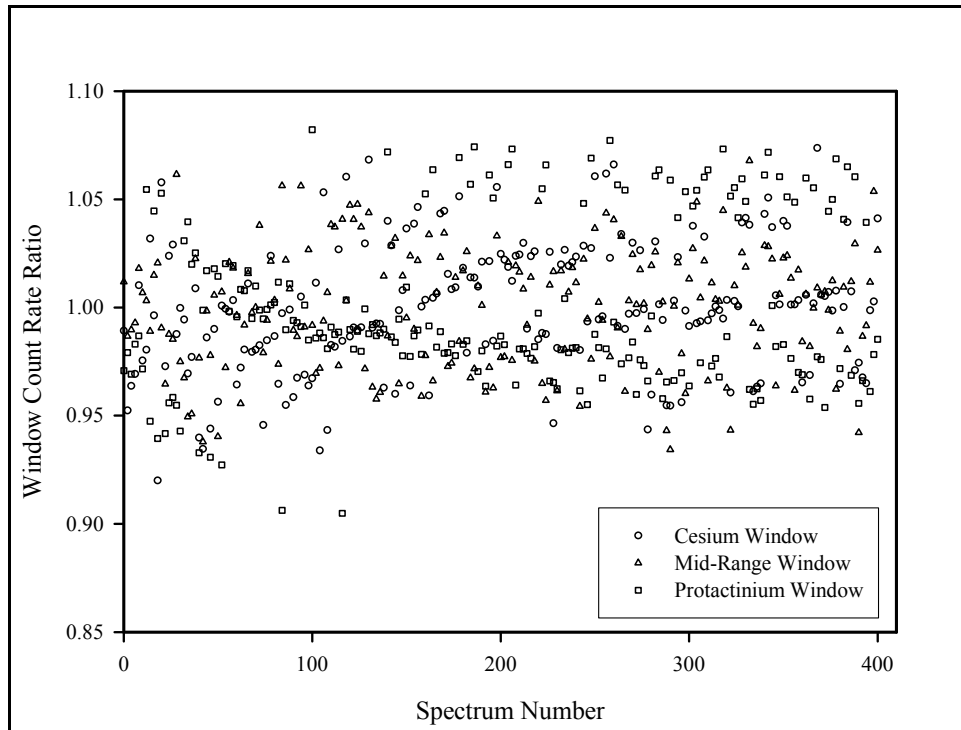


Figure 3-9. Stability of Cesium, Mid-Range, and Protactinium Window Count Rates when Window Settings are Adjusted for Gain Shift

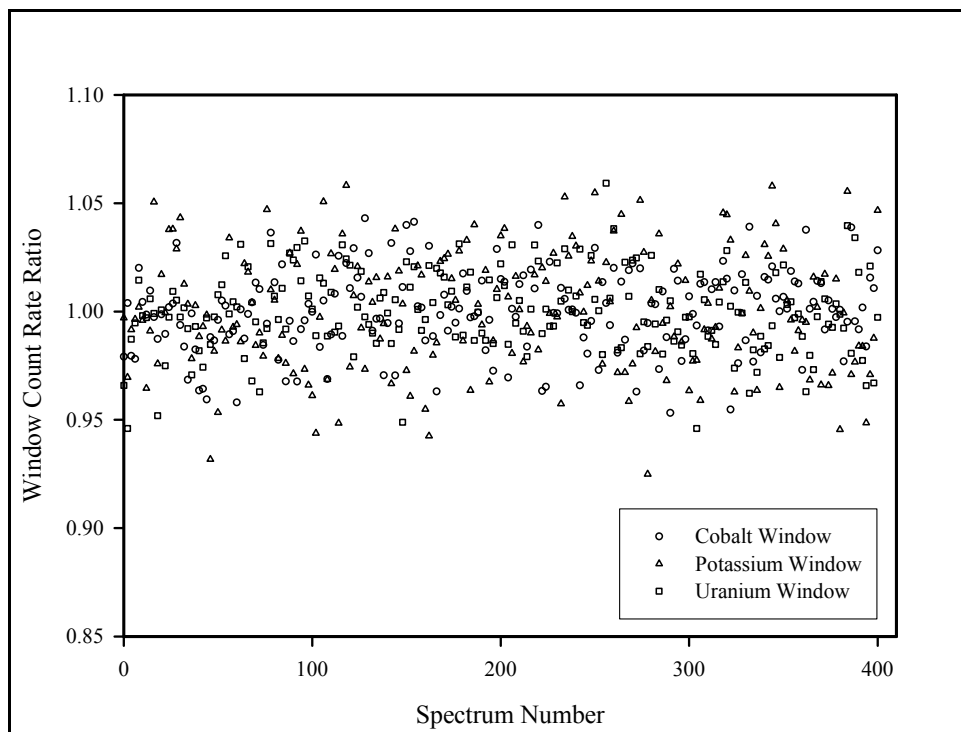


Figure 3-10. Stability of Cobalt, Potassium, and Uranium Window Count Rates when Window Settings are Adjusted for Gain Shift

As indicated by the plot in Figure 3-11, the thorium window count rate ratio decreased as the stability test progressed. With each upward shift of system gain, the thorium window shrank in

width because the lower window boundary moved to a higher channel number while the upper boundary remained fixed (at channel 255). Simultaneously, counts for the photons with the highest energies were lost. Pulse heights for pulses corresponding to these photons exceeded the pulse height corresponding to channel 255, and the system did not register counts for these pulses. In other words, when gain shift moved the upper end of the spectrum off scale, the counts in the off scale portion were lost.

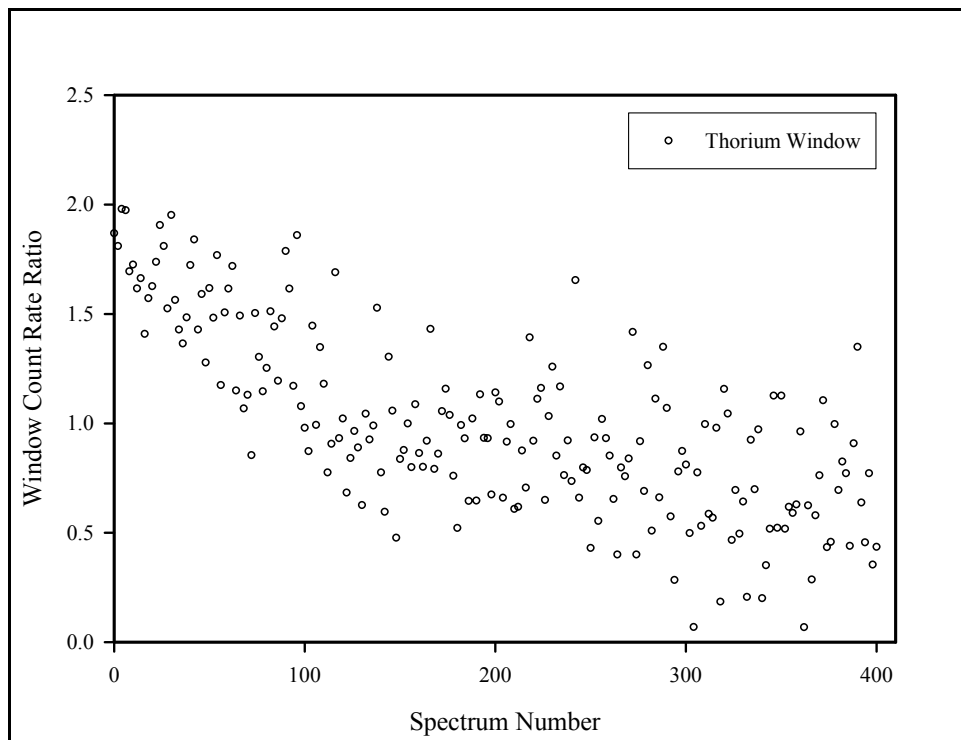


Figure 3-11. Stability of Thorium Window Count Rates when Window Settings are Adjusted for Gain Shift

The statistical scatter in the data points in Figure 3-11 is due to the small number of counts captured by the thorium window.

### 3.3.1.1 Addendum to the Large Detector Stability Test

The power supply within the sonde generated heat that dissipated slowly when the sonde was centered in an air-filled hole. Consequently, the temperature of the electronic components within the sonde probably increased significantly during the 5-hour test. The test period also happened to include the time of day when the highest air temperature probably occurred. The temperature of the sonde could not be monitored during the test, but the sonde most likely heated gradually as the test progressed. The system gain drifted consistently upward during the test, suggesting that the temperature change and the gain shift might be linked.

In July 2002, the power supply in the sonde was replaced with a power supply mounted in the surface electronics. Removal of the main source of heat generation from the sonde would presumably improve the temperature stability. However, a repeat of the stability test did not

indicate that the gain stability was improved.

The second stability test was conducted on August 6, 2002. The sonde was placed in the SBA standard and two sets of spectra were acquired without disturbing the sonde. The first set had 209 spectra (STAB1000.CHN through STAB1208.CHN) that were recorded from 5:26 AM to 8:03 AM. The second set had 174 spectra (STAB2000.CHN through STAB2173.CHN) that were recorded from 8:15 AM to 10:25 AM. Spectral data analogous to those displayed in Figure 3-7 appear in Figure 3-12.

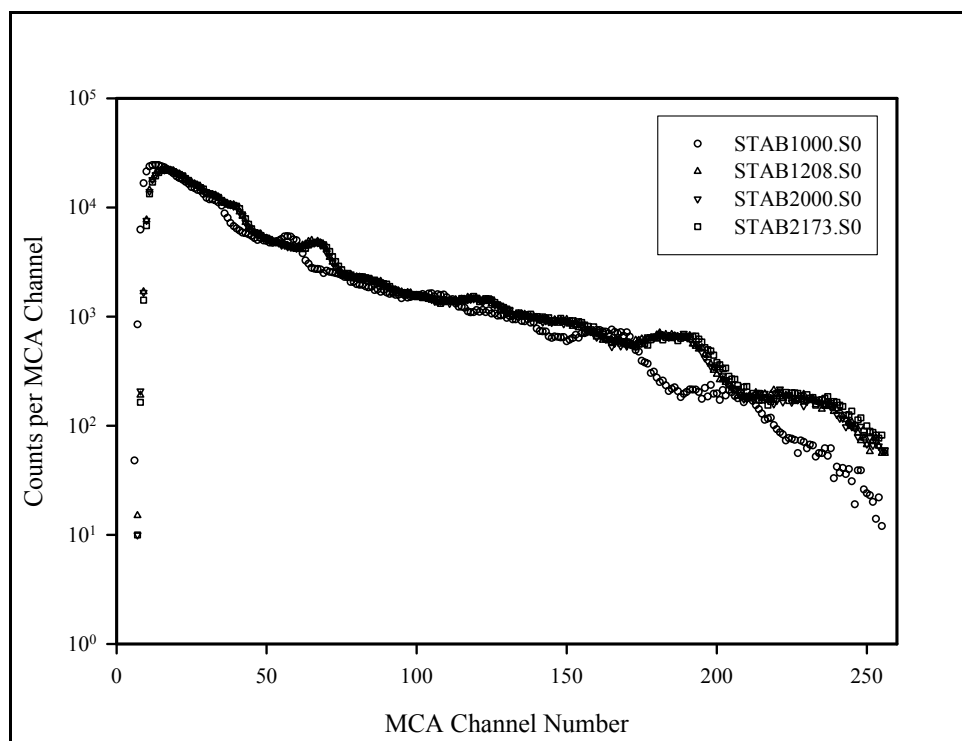


Figure 3-12. Stability Test after Power Supply Replacement

Comparison of the spectra in Figure 3-12 with the spectra in Figure 3-7 indicates that the upward shift in gain in the second test was almost identical to the gain shift observed in the first test. In the second test, the two spectra collected near the middle of the test (spectra STAB1208.CHN and STAB2000.CHN) nearly coincide with the spectrum collected at the end of the test (spectrum STAB2173.CHN), indicating that most of the gain shift occurred during the first part of the test.

Figure 3-13 shows data analogous to those shown in Figure 3-2. The efficiency, as gauged by the total count rate, climbed steadily during the second test, following the same pattern as the first test. Each efficiency value measured in the second test was lower than the analogous value from the first test.

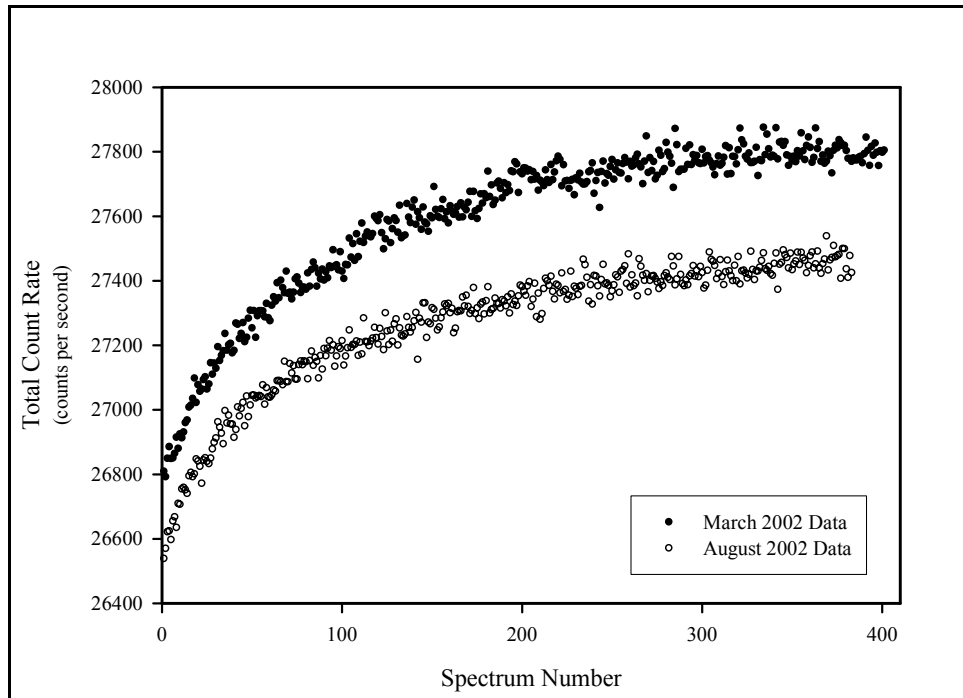


Figure 3-13. Comparison of Efficiency Changes over Time

For the spectra from the first and second tests, efficiency ratios were calculated by dividing the total count in spectrum number N from the first test by the total count in spectrum number N from the second test. The efficiency ratios are plotted in relation to spectrum numbers in Figure 3-14.

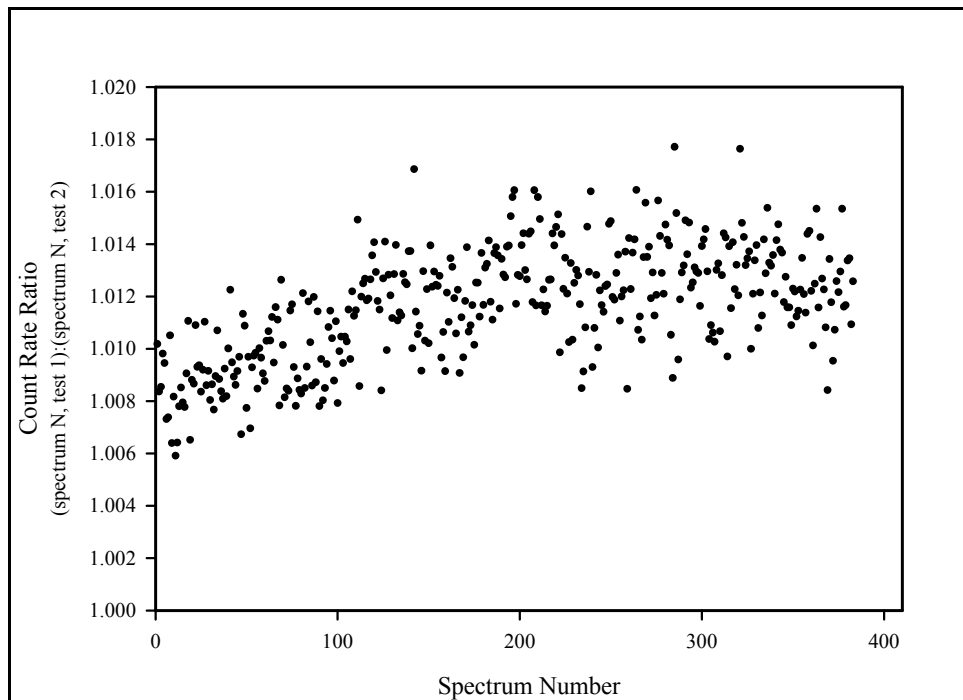


Figure 3-14. Relative Efficiency Changes over Time

For each spectrum, a count rate ratio, defined as the count rate in the spectrum divided by the average count rate for all of the spectra, was calculated. In Figure 3-15, count rate ratios for the two tests are plotted in relation to spectrum number. Over the test durations, the count rates increased by about 3.5 percent in both cases. In both tests, the rate of change of count rate was highest at the beginning, and the rate of change gradually decreased.

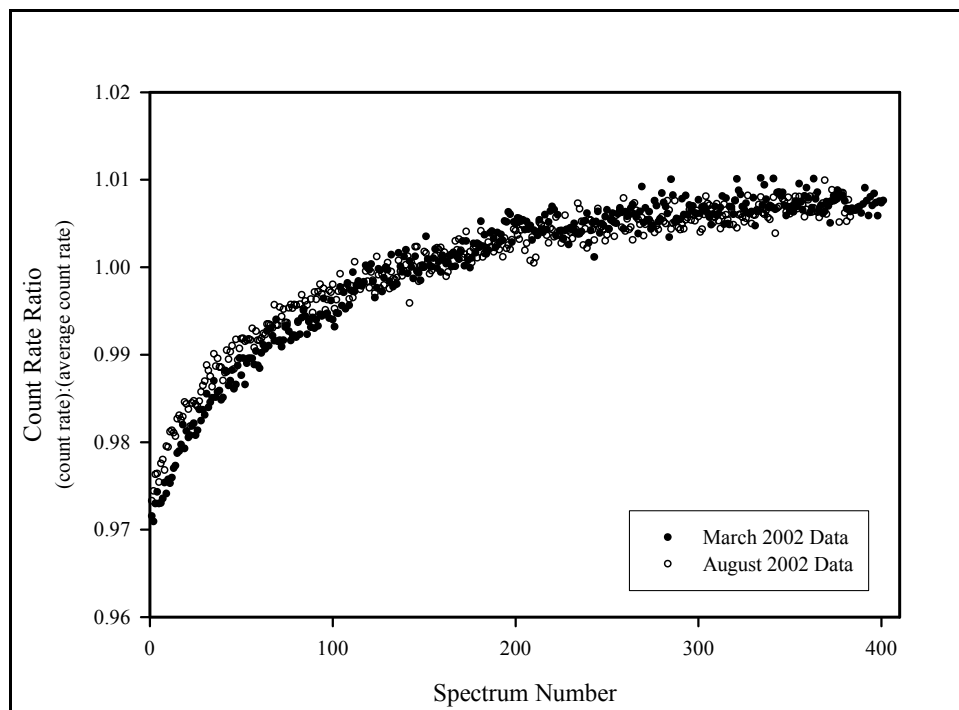


Figure 3-15. Relative Changes in Count Rate over Time

### 3.3.2 Small Detector Stability Tests

Gain shifts as drastic as those observed with the large detector did not occur with the small and medium detectors. Although the photomultiplier tubes for the small and medium detectors were shielded from magnetic fields by mu-metal, and the tube for the large detector was unshielded, the shields are unlikely to account for the gain stability because there were no known experimental factors that could have generated changing magnetic fields near the large detector photomultiplier.

For the stability test conducted with the small detector, the sonde was placed at the center of the SBH calibration standard (Appendix A) and 233 spectra (SHUBL000.CHN through SHUBL232.CHN) were recorded, with a 30-second acquisition time per spectrum, without moving or otherwise disturbing the sonde. After a short pause (approximately 5 minutes), 336 additional spectra (SHUBM000.CHN through SHUBM335.CHN) were recorded at 30 seconds per spectrum. Data acquisition began at 8:07 AM on March 7, 2002, and ended at about 2:09 PM.

Figures 3-16 and 3-17 illustrate the gain stability that characterized the SHUBL\*\*\*.S0 series spectra and the SHUMB\*\*\*.S0 series spectra.

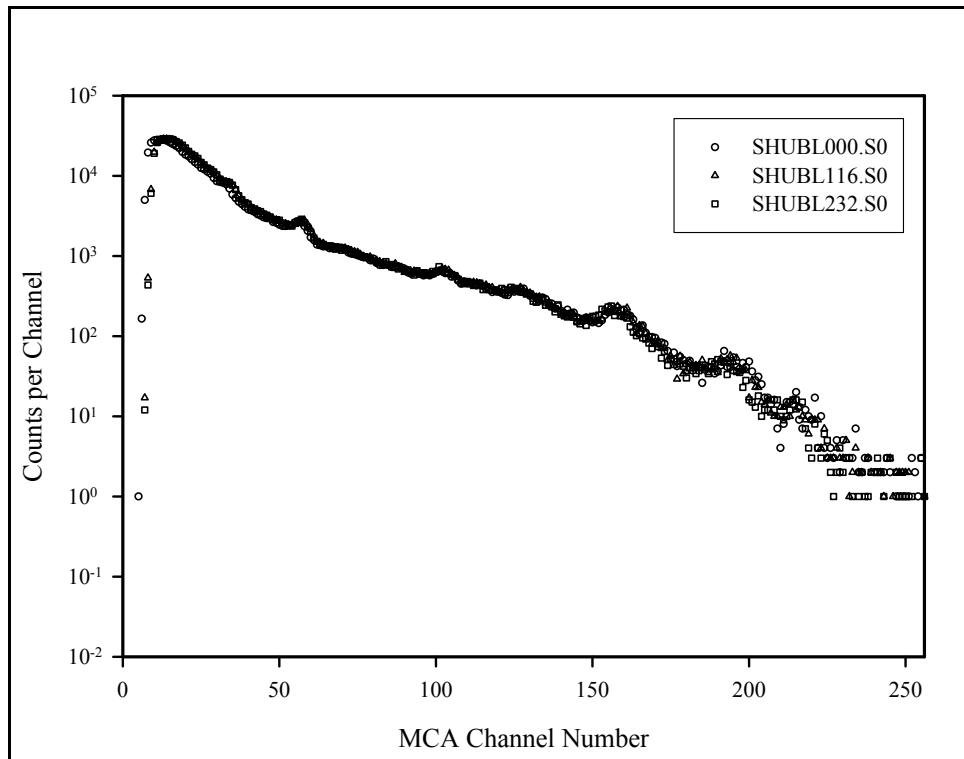


Figure 3-16. First Small Detector Gain Stability Test

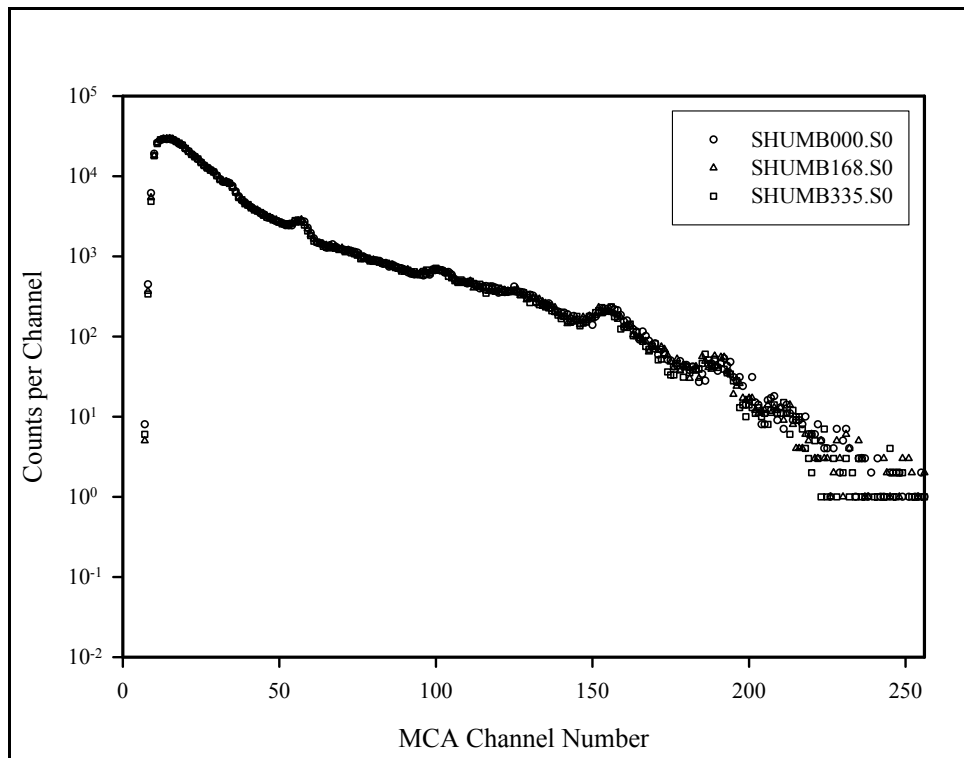


Figure 3-17. Second Small Detector Gain Stability Test

There was little gain shift during the collection of the 233 spectra in the SHUBL\*\*\*.S0 series, or during the collection of the 336 spectra in the SHUMB\*\*\*.S0 series. However, the total gain shift, from the start of the first acquisition to the end of the second acquisition, was not negligible, as indicated by the spectra plotted in Figure 3-18.

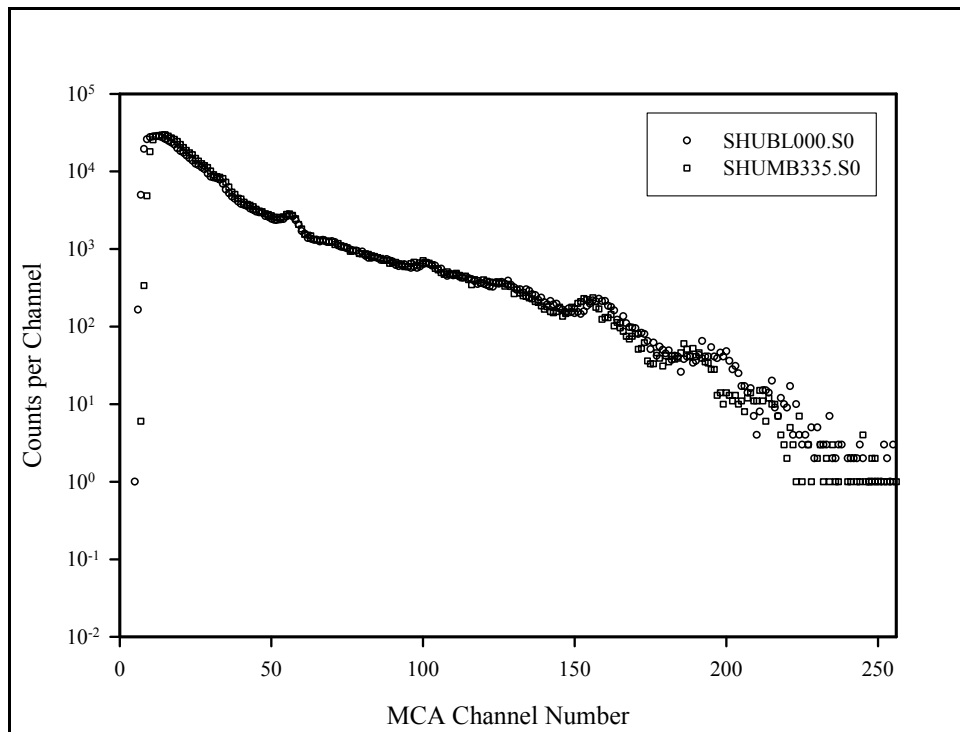


Figure 3-18. Gain Shift During Small Detector Stability Test

During the test, the center of the peak for the 1764.5-keV gamma ray migrated as indicated in Table 3-1.

Table 3-1. Position of the 1764.5-keV Gamma-Ray Peak during the Small Detector Stability Test

Spectrum Name	1764.5-keV Gamma-Ray Peak Center (MCA channel number)
SHUBL000.S0	160
SHUBL115.S0	157
SHUBL231.S0	155
SHUBM000.S0	155
SHUBM168.S0	154
SHUBM335.S0	154

The net shift of 6 channels corresponded to an energy change of about 68 kilo-electron-volts. In these particular tests, the shift was toward lower gain, which was opposite to the trend observed for the large detector test. This is additional evidence that the gain shift was not driven by temperature change.

The efficiency changed during both acquisitions. During the acquisition of the SHUBL\*\*\*.CHN series spectra, the efficiency drifted upward by a bit less than 1 percent; the efficiency drifted downward by a bit less than 1 percent during the acquisition of the SHUBM\*\*\*.CHN series. These trends are shown by the total count rate data plotted in Figure 3-19. The vertical axis has the same count ratio scale as used in Figure 3-3. Comparison of the graphs in Figures 3-3 and 3-19 indicates that the relative efficiency change for the small detector was much smaller than for the large detector.

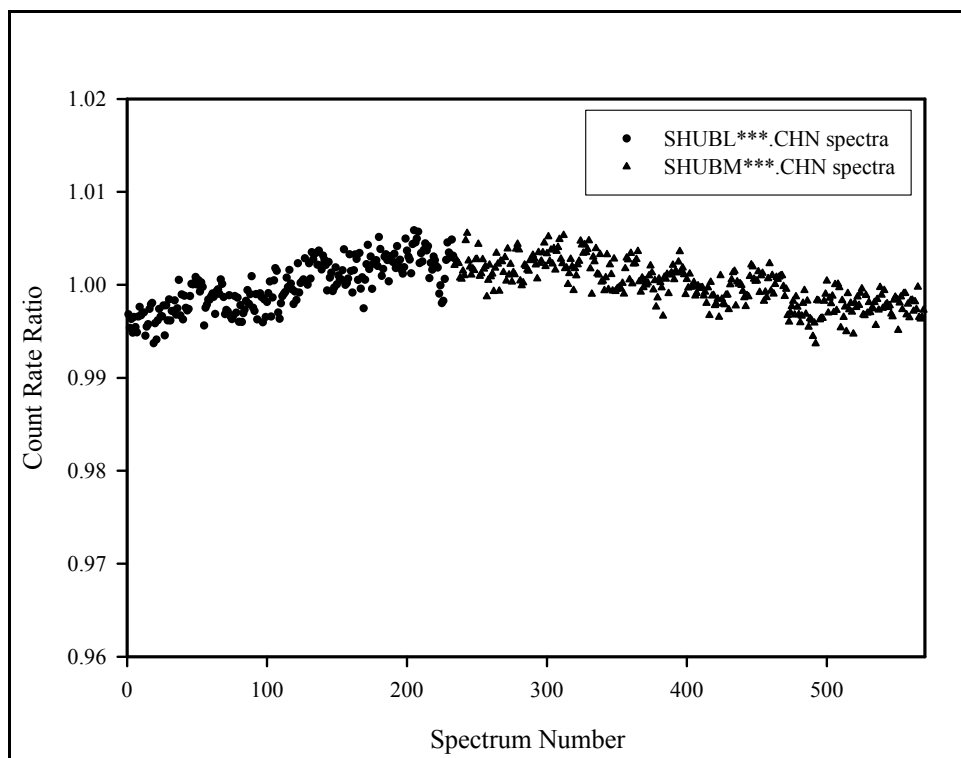


Figure 3-19. Relative Change in Efficiency during Small Detector Stability Test

### 3.3.3 Medium Detector Stability Tests

With the medium detector, three groups of stability test data were recorded on March 8, 2002: 163 spectra named MMUBO\*\*\*.CHN were acquired at 30 seconds per spectrum with the sonde centered in standard SBM, 36 spectra, named MMUBP\*\*\*.CHN, were acquired with the same acquisition parameters, and 191 spectra, named MMUBQ\*\*\*.CHN, were acquired with the same acquisition parameters. Data acquisition began at about 5:29 AM and ended at about 9:41 AM. There were two time gaps of approximately 5 minutes each between the MMUBO and MMUBP groups, and between the MMUBP and MMUBQ groups.

The medium detector gain was essentially stable during the tests, as indicated by the overlap of the two spectra in Figure 3-20. MMUBO000.S0 was the first spectrum from the MMUBO group, and MMUBQ190.S0 was the last spectrum from the MMUBQ group.

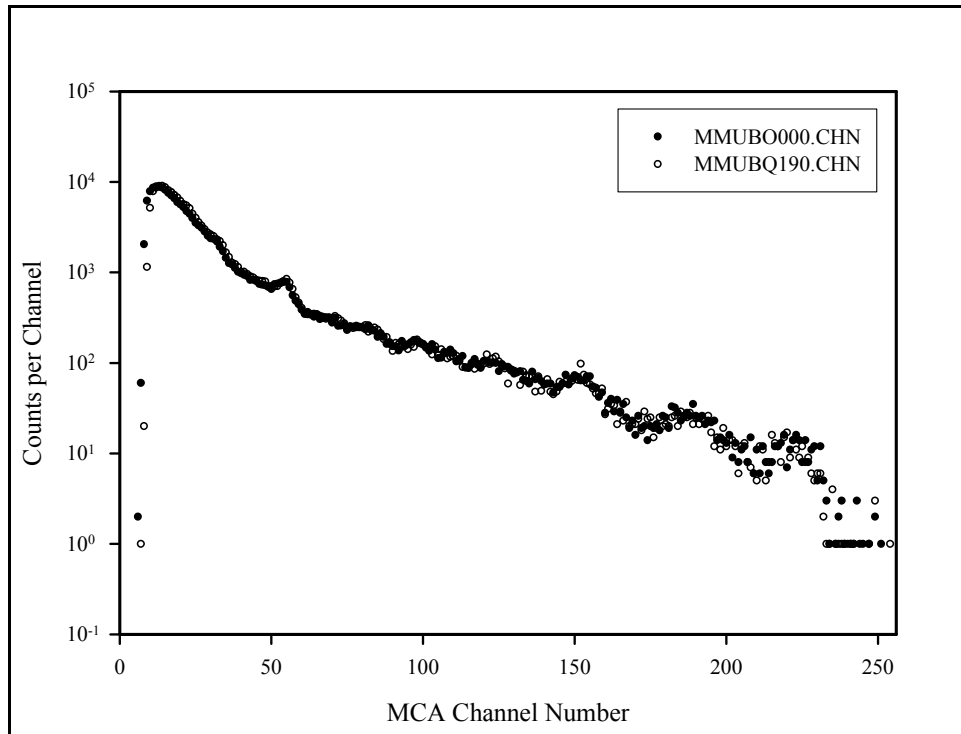


Figure 3-20. Gain Shift during Medium Detector Stability Test

Data in Table 3-2 show how the center of the 1764.5-keV gamma-ray peak migrated during the test.

Table 3-2. Position of the 1764.5-keV Gamma-Ray Peak during the Medium Detector Stability Test

Spectrum Name	1764.5-keV Gamma-Ray Peak Center (MCA channel number)
MMUBO000.S0	151
MMUBO081.S0	151
MMUBO161.S0	151
MMUBP001.S0	154
MMUBP018.S0	148
MMUBP035.S0	153
MMUBQ000.S0	152
MMUBQ095.S0	152
MMUBQ190.S0	150

The 1764.5-keV gamma-ray peak was indistinct in these spectra and the spectrum analysis program could not consistently delineate the peak. Most likely, the gain was essentially stable and the apparent migration of the peak center was an artifact of inconsistent peak fitting by the spectrum analysis program.

The medium detector was comparable to the small detector in efficiency stability. Figure 3-21 displays the total count ratios from the stability test data (spectral sets MMUBO, MMUBP, and MMUBQ). The efficiency might have drifted slightly downward during the data acquisitions, but if so, the net change was only a few tenths of a percent.

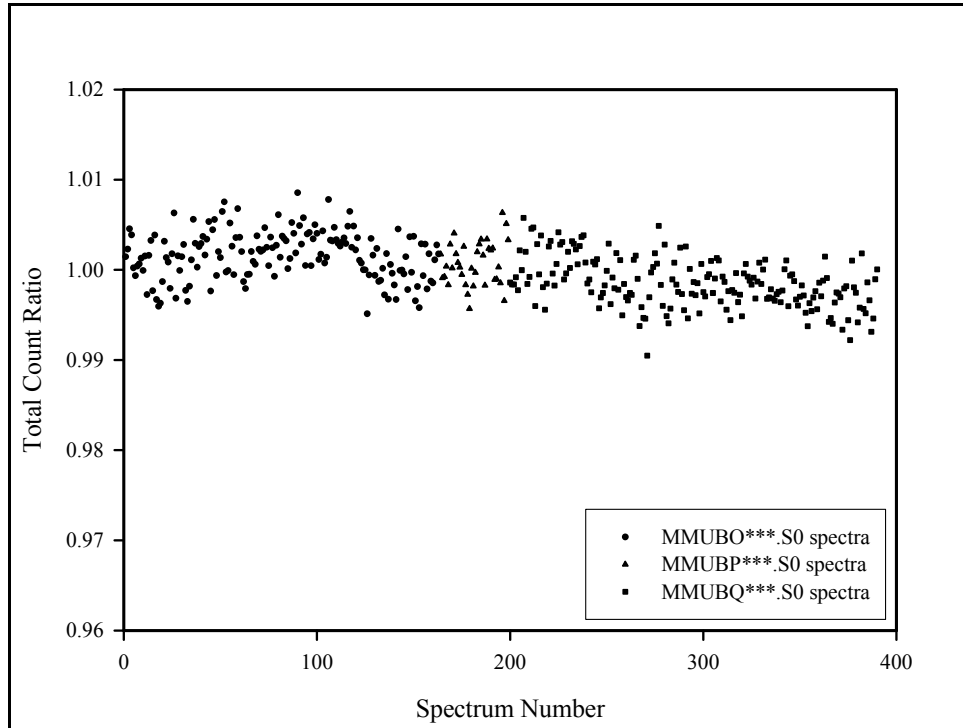
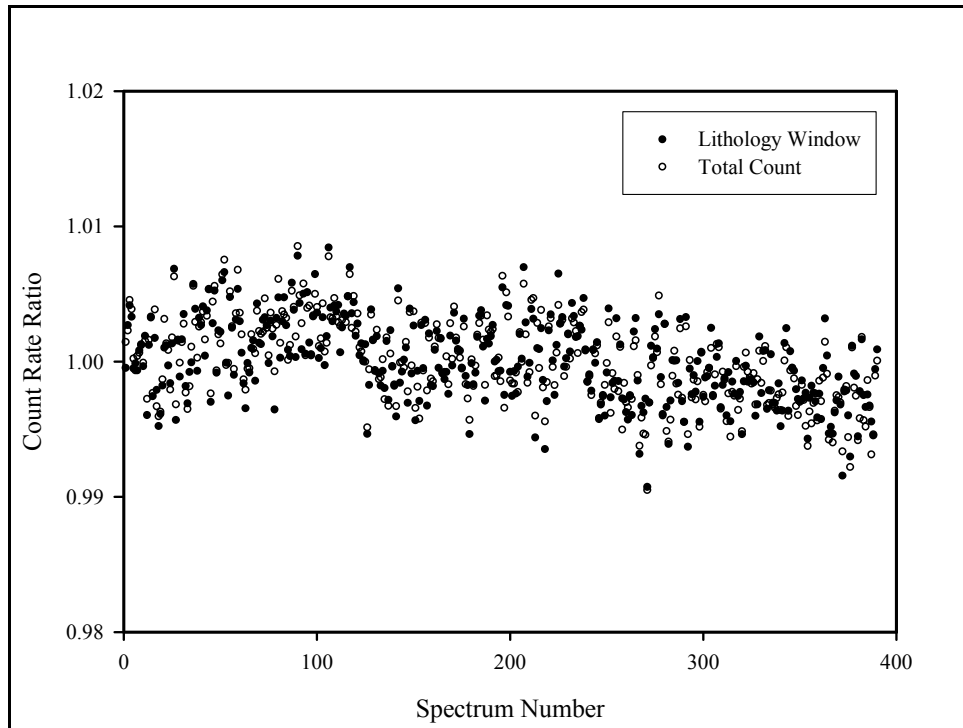


Figure 3-21. Relative Change in Efficiency during Medium Detector Stability Test

The count rates in the lithology window followed the same trend as the total count rate, as indicated by the plot in Figure 3-22.



*Figure 3-22. Relative Change in Lithology Window Count Rate during Medium Detector Stability Test*

If the gain and efficiency were nearly stable, there should be no upward or downward trends in the various window count rates. Two examples, cesium window count rates and cobalt window count rates, are presented in Figure 3-23 to support this contention.

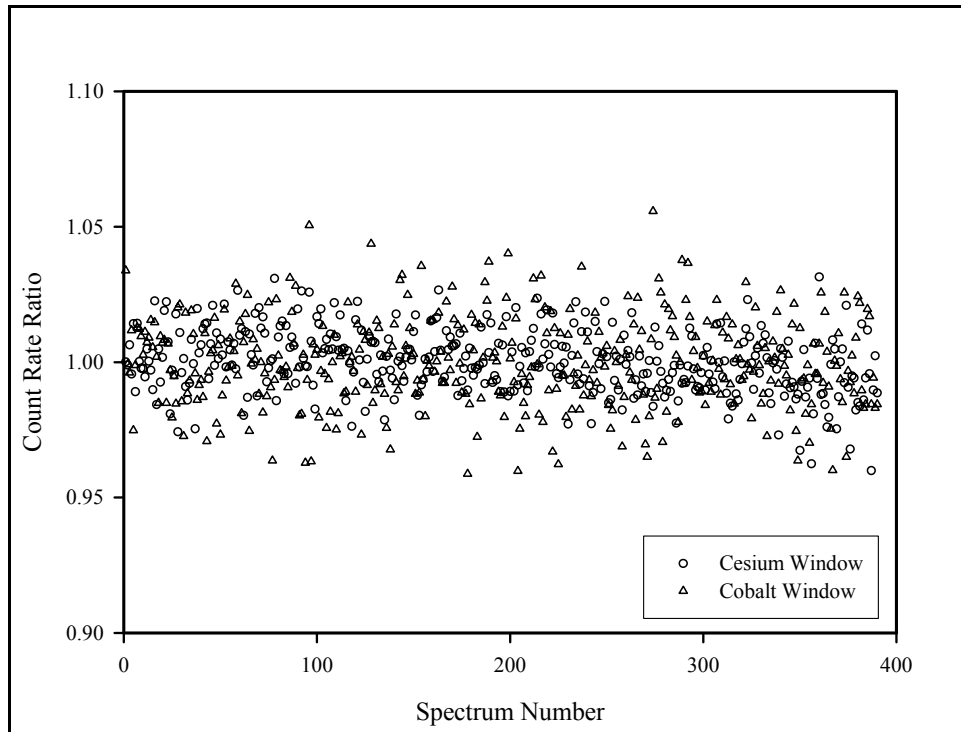


Figure 3-23. Relative Changes in Cesium and Cobalt Window Count Rates during Medium Detector Stability Test

Thorium window data are displayed in Figure 3-24. The data in Figure 3-24, and in previous figures, might appear to have extreme fluctuations. “Error bars” showing  $2\sigma$  counting uncertainties have been placed on every tenth datum to show that statistical counting fluctuations account for the scatter.

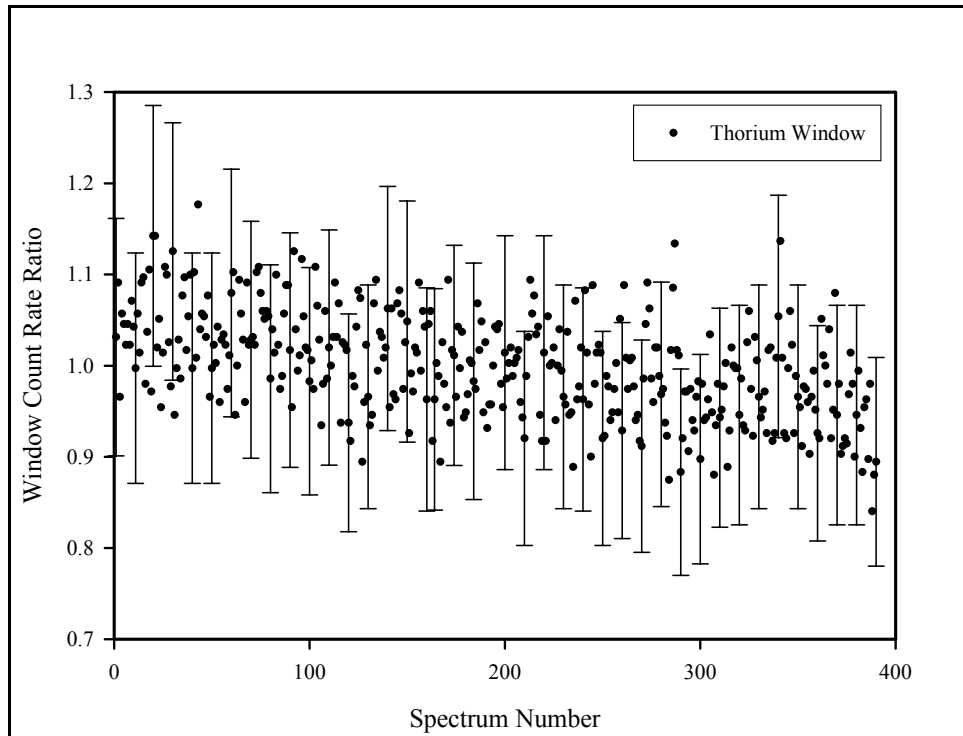


Figure 3-24. Relative Changes in Thorium Window Count Rates during Medium Detector Stability Test

### 3.3.4 Recommendations

The large detector stability test data indicate that when the spectral windows are fixed at specific MCA channel numbers, gain shift can effect significant changes in window count rates, though the source intensity is constant (within radioactive decay fluctuations). A seemingly obvious remedy, to energy-calibrate each spectrum then set windows by energy, is largely impractical for several reasons. There is no way to automate the energy calibration with the analysis software. Manual energy calibration is far too time-intensive, and there are usually no reliable peaks to use as energy references in the field spectra because the full energy peaks tend to be broad and indistinct.

The logging engineers have developed and implemented the following procedure to minimize gain shifts caused by temperature changes.

- After the equipment is in place to log a borehole, the sonde electronic components are allowed to warm up for 30 minutes before the pre-survey field verification spectrum is acquired.
- The sonde is lowered into the borehole and allowed to adjust to the temperature, then the gain is reset and a gain check spectrum is acquired.
- The borehole log is recorded.

- A post-survey gain check spectrum is acquired at the end of the logging run so that the gain drift can be measured.

A borehole is typically logged in about an hour, and the gain drift over this short time is usually minimal. However, if a data analyst notices that the gain shift in a set of spectra is not negligible, the analyst should not analyze all of the spectra in one *Supervisor* run. Instead, the set should be divided into smaller sets within which the gain shifts are minor, and the spectra in each subset should be analyzed with *Supervisor*, with window settings appropriate for the subset.

Gain shifts could probably be greatly reduced by retrofitting an effective electronic gain stabilization module on the system. This would solve many problems and thus deserves consideration.

## 4.0 Calibration Measurements

### 4.1 Data Acquisition

Calibration data were acquired using the borehole calibration standards at the Hanford calibration facility. Appendix A provides details about these standards. Six spectra were recorded with each standard. Details about the measurements are summarized in Table 4-1.

Each calibration spectrum was recorded with the detector held stationary at the (vertical) center of a borehole calibration standard. The sonde was centralized in the test hole, and there was no liquid in the test hole. Test holes in the calibration standards do not have casing, but a “steel sleeve” (section of 0.28-inch-thick steel pipe) can be mounted on the sonde to simulate the effect of the most common borehole casing at Hanford, which is steel pipe with a diameter (inner) of 6.0 inches and a wall thickness of 0.28 inch.

Table 4-1. Calibration Measurement Details

Detector	Steel Sleeve	Standards	Counting Time per Spectrum (seconds)	Number of Spectra
Small	no	SBM, SBL, SBB, SBH	600	6 per standard
Medium	no	SBK, SBM, SBL, SBB, SBH	300	
	yes	SBB, SBH		
Large	no	SBK, SBA, SBT, SBM, SBU	200	

For the calibration spectra, counts and count rates were calculated for the eight spectral windows shown in Table 2-2.

For routine analysis of log data, window counts and count rates are calculated using two algorithms in the Aptec Engineering spectrum analysis program set. First, a field verification spectrum is energy-calibrated with the *PCMCA/WIN* spectrum analysis algorithm, and the energy calibration is used to establish the MCA channel numbers corresponding to the seven adjustable spectral window boundaries. Next, sets of spectra are batch-processed by the *Supervisor* algorithm, which is programmed to “import” the window settings to each spectrum, then calculate the counts in each window by summing the counts in the channels within the window.

The calibration spectra were not analyzed by the routine method because *Supervisor* sets windows by MCA channel number instead of energy. This is not the preferred way to set windows if the logging system is susceptible to gain shift. If multiple calibration spectra are acquired using a particular calibration standard, the counts in any window should be constant, within counting statistics. However, gain shift during the acquisition will cause the counts in a window to vary, even though the gamma-ray source intensity is constant.

Effects of gain shifts on window counts were minimized by setting window boundaries by energy instead of channel number. To do this, each calibration spectrum was opened with *PCMCA/WIN*, and the pre-set energy calibration was checked by observing the energies assigned

to the 609.3-keV and 1764.5-keV “uranium” gamma-ray peaks. If the energies were in error by more than a couple of kilo-electron-volts, the spectrum was recalibrated for energy, using the 609.3-keV and 1764.5-keV gamma-ray peaks as calibration references. The *save as* command was then executed with the *channel data (\*.CSV)* file type specified. This saved the spectrum as a Microsoft® *Excel* spreadsheet file with three columns of data containing channel numbers, energies, and counts, respectively.

In each *Excel* file, the window boundaries were set manually by energy instead of channel number. With *Excel* programming, the sum of counts over MCA channels within each window was calculated, and the window count rate was derived by dividing the window counts by the live spectrum acquisition time. For each group of spectra from a particular calibration standard, average count rates were calculated for each window. These average window count rates are displayed in Tables 4-2, 4-3, and 4-4.

Table 4-2. Calibration Count Rate Data for the Small Detector

Window Names and Count Rates in Counts per Second									
Standard	Lithology	Cs-137	Mid-Range	Pa-234	Co-60	K-40	U-238	Th-232	Total
SBM	1191.1 ± 4.2	46.73 ± 0.38	27.21 ± 0.54	11.55 ± 0.29	20.70 ± 0.40	8.01 ± 0.14	12.43 ± 0.38	1.22 ± 0.05	1319.0 ± 4.3
SBL	2383.3 ± 5.0	98.7 ± 1.2	55.37 ± 0.74	23.51 ± 0.45	45.54 ± 0.50	16.47 ± 0.58	19.05 ± 0.31	0.51 ± 0.04	2642.5 ± 5.8
SBB	6236 ± 20	266.9 ± 2.7	152.8 ± 1.9	64.97 ± 0.63	126.4 ± 0.2	43.53 ± 0.60	51.56 ± 0.85	1.39 ± 0.14	6943 ± 21
SBH	18081 ± 33	954.5 ± 3.9	563.2 ± 3.3	241.7 ± 1.7	454.5 ± 2.0	158.6 ± 3.6	195.8 ± 5.9	7.14 ± 0.52	20657 ± 26

Table 4-3. Calibration Count Rate Data for the Medium Detector

Window Names and Count Rates in Counts per Second									
Standard	Lithology	Cs-137	Mid-Range	Pa-234	Co-60	K-40	U-238	Th-232	Total
SBK	136.7 ± 1.9	8.63 ± 0.32	6.25 ± 0.28	3.42 ± 0.25	6.58 ± 0.31	4.39 ± 0.29	0.563 ± 0.094	0.051 ± 0.026	166.6 ± 1.8
SBM	5000 ± 22	278.6 ± 3.1	148.1 ± 1.2	64.74 ± 0.90	120.9 ± 1.3	46.64 ± 0.84	77.6 ± 1.8	11.05 ± 0.42	5748 ± 26
SBL	9891.4 ± 9.8	586.1 ± 3.8	298.7 ± 1.2	127.2 ± 1.9	276.2 ± 1.8	94.74 ± 0.89	130.53 ± 0.92	4.83 ± 0.28	11409.7 ± 9.7
SBB	24368 ± 25	1720.4 ± 4.3	930.6 ± 4.8	398.3 ± 3.3	833.8 ± 3.0	294.6 ± 2.0	419.0 ± 2.8	21.66 ± 0.76	28987 ± 30
SBB (S) <sup>1</sup>	17341 ± 29	1208.0 ± 7.5	668.6 ± 3.7	288.1 ± 3.2	601.2 ± 2.0	207.7 ± 3.3	292.1 ± 3.3	13.49 ± 0.42	20620 ± 19
SBH	54526 ± 74	6504 ± 12	4078 ± 14	1795.5 ± 5.3	3545 ± 13	1347.0 ± 9.4	2152 ± 16	230.5 ± 3.6	74179 ± 128
SBH (S)	44243 ± 43	4595 ± 90	2822 ± 40	1242 ± 13	2464 ± 22	915.8 ± 7.5	1412 ± 15	127.3 ± 1.7	57820 ± 206

<sup>1</sup>(S) indicates that the steel sleeve was installed during the measurements.

Table 4-4. Calibration Count Rate Data for the Large Detector

Window Names and Count Rates in Counts per Second									
Standard	Lithology	Cs-137	Mid-Range	Pa-234	Co-60	K-40	U-238	Th-232	Total
SBK	1494.9 ± 2.9	160.1 ± 1.5	125.1 ± 1.0	66.94 ± 0.80	140.8 ± 1.7	153.8 ± 2.7	17.75 ± 0.59	1.91 ± 0.26	2161.4 ± 4.1
SBA	19660 ± 57	2274 ± 21	1343.8 ± 6.9	598.2 ± 8.7	1326 ± 13	581.5 ± 6.1	970 ± 34	85.7 ± 6.7	26840 ± 67
SBT	22368 ± 112	2742 ± 89	1932 ± 13	1041 ± 58	1193 ± 94	524.5 ± 4.9	1332 ± 18	669 ± 24	31801 ± 108
SBM	42119 ± 64	6162 ± 39	4376 ± 23	2025 ± 15	3825 ± 21	1731 ± 13	3273 ± 42	740 ± 16	64252 ± 121
SBU	45643 ± 115	6896 ± 144	4775 ± 93	2205 ± 28	4613 ± 86	2043 ± 63	3686 ± 201	430 ± 61	70291 ± 571

Tables 4-5 and 4-6 show small detector count rate data for particular calibration standards, to allow comparison of the 2002 data with data acquired for the previous (2000) calibration.

Table 4-5. Small Detector 2002 Count Rate Data (no sleeve)

Window Names and Count Rates in Counts per Second									
Standard	Lithology	Cs-137	Mid-Range	Pa-234	Co-60	K-40	U-238	Th-232	Total
SBL	2383.3 ± 5.0	98.7 ± 1.2	55.37 ± 0.74	23.51 ± 0.45	45.54 ± 0.50	16.47 ± 0.58	19.05 ± 0.31	0.51 ± 0.04	2642.5 ± 5.8
SBB	6236 ± 20	266.9 ± 2.7	152.8 ± 1.9	64.97 ± 0.63	126.4 ± 0.2	43.53 ± 0.60	51.56 ± 0.85	1.39 ± 0.14	6943 ± 21
SBH	18081 ± 33	954.5 ± 3.9	563.2 ± 3.3	241.7 ± 1.7	454.5 ± 2.0	158.6 ± 3.6	195.8 ± 5.9	7.14 ± 0.52	20657 ± 26

Table 4-6. Small Detector 2000 Count Rate Data (no sleeve)

Window Names and Count Rates in Counts per Second									
Standard	Lithology	Cs-137	Mid-Range	Pa-234	Co-60	K-40	U-238	Th-232	Total
SBL	2186.8 ± 7.4	100.2 ± 2.8	60.7 ± 1.1	23.99 ± 0.94	46.88 ± 0.75	16.82 ± 0.54	17.94 ± 0.22	0.448 ± 0.029	2435. ± 6.6
SBB	5757.4 ± 9.2	281.4 ± 5.4	165.7 ± 3.6	66.8 ± 2.6	132.7 ± 2.1	46.85 ± 0.94	51.29 ± 0.44	1.337 ± 0.062	6450.0 ± 7.3
SBH	16303 ± 94	986 ± 29	606 ± 17	247 ± 11	467.0 ± 8.7	167.6 ± 3.7	189.7 ± 2.1	6.54 ± 0.29	18775 ± 98

Tables 4-7 and 4-8 show medium detector count rate data for particular calibration standards, to allow comparison of the 2002 data with data acquired for the previous (2000) calibration.

Table 4-7. Medium Detector 2002 Count Rate Data

Window Names and Count Rates in Counts per Second									
Standard	Lithology	Cs-137	Mid-Range	Pa-234	Co-60	K-40	U-238	Th-232	Total
SBL	9891.4 ± 9.8	586.1 ± 3.8	298.7 ± 1.2	127.2 ± 1.9	276.2 ± 1.8	94.74 ± 0.89	130.53 ± 0.92	4.83 ± 0.28	11409.7 ± 9.7
SBB	24368 ± 25	1720.4 ± 4.3	930.6 ± 4.8	398.3 ± 3.3	833.8 ± 3.0	294.6 ± 2.0	419.0 ± 2.8	21.66 ± 0.76	28987 ± 30
SBH	54526 ± 74	6504 ± 12	4078 ± 14	1795.5 ± 5.3	3545 ± 13	1347.0 ± 9.4	2152 ± 16	230.5 ± 3.6	74179 ± 128

Table 4-8. Medium Detector 2000 Count Rate Data (no sleeve)

Window Names and Count Rates in Counts per Second									
Standard	Lithology	Cs-137	Mid-Range	Pa-234	Co-60	K-40	U-238	Th-232	Total
SBL	8959 ± 84	590 ± 18	325.7 ± 3.0	134.5 ± 6.5	276.3 ± 2.5	97.8 ± 2.7	127.8 ± 1.0	4.43 ± 0.19	10401 ± 76
SBB	22127 ± 28	1733 ± 32	998 ± 24	426 ± 21	826 ± 19	292 ± 10	398.5 ± 3.5	17.32 ± 0.52	26467 ± 32
SBH	49887 ± 225	6098 ± 187	4029 ± 37	1772.8 ± 8.2	3142 ± 43	1183 ± 17	1479 ± 59	77.1 ± 5.7	66414 ± 275

Tables 4-9 and 4-10 show large detector count rate data for particular calibration standards, to allow comparison of the 2002 data with data acquired for the previous (2000) calibration.

Table 4-9. Large Detector 2002 Calibration Count Rate Data

Window Names and Count Rates in Counts per Second									
Standard	Lithology	Cs-137	Mid-Range	Pa-234	Co-60	K-40	U-238	Th-232	Total
SBK	1494.9 ± 2.9	160.1 ± 1.5	125.1 ± 1.0	66.94 ± 0.80	140.8 ± 1.7	153.8 ± 2.7	17.75 ± 0.59	1.91 ± 0.26	2161.4 ± 4.1
SBT	22368 ± 112	2742 ± 89	1932 ± 13	1041 ± 58	1193 ± 94	524.5 ± 4.9	1332 ± 18	669 ± 24	31801 ± 108
SBM	42119 ± 64	6162 ± 39	4376 ± 23	2025 ± 15	3825 ± 21	1731 ± 13	3273 ± 42	740 ± 16	64252 ± 121
SBU	45643 ± 115	6896 ± 144	4775 ± 93	2205 ± 28	4613 ± 86	2043 ± 63	3686 ± 201	430 ± 61	70291 ± 571

Table 4-10. Large Detector 2000 Calibration Count Rate Data

Window Names and Count Rates in Counts per Second									
Standard	Lithology	Cs-137	Mid-Range	Pa-234	Co-60	K-40	U-238	Th-232	Total
SBK	1406 ± 24	155 ± 10	125.9 ± 4.5	67.4 ± 5.1	152.0 ± 9.3	138.5 ± 8.4	16.39 ± 0.39	1.62 ± 0.10	2062 ± 24
SBT	21820 ± 110	2172 ± 33	1845.0 ± 3.4	725 ± 31	1081.7 ± 8.5	530.3 ± 3.1	1282.8 ± 2.3	466 ± 23	29923 ± 154
SBM	40482 ± 54	5478 ± 59	4050 ± 30	2001 ± 14	3969 ± 22	1649 ± 12	3165 ± 21	618.0 ± 7.2	61411 ± 172
SBU	43977 ± 794	5929 ± 335	4304 ± 156	2154 ± 37	4680 ± 163	1881 ± 103	3359 ± 351	305 ± 66	66590 ± 502

## 4.2 Use of Calibration Data

As indicated in Section 1.0, RAS calibrations do not produce formulas for calculating radionuclide concentrations from spectral data. The purpose of calibration is to periodically check and monitor the system efficiency, gain, and other performance characteristics. If total count rate is a measure of efficiency, this calibration indicated that the efficiencies increased by about 9 percent for the small detector, 10 percent for the medium detector, and 5 percent for the large detector, relative to the previous calibration. The small and medium detectors have nearly stable gains, but sizable gain shifts of unknown origin continue to afflict the large detector. Measurements using the SBA calibration source showed that the gain shifts can cause significant changes in window count rates if data analysis is based on windows that have boundaries fixed at specific MCA channel numbers.

A major barrier to the development of data analysis for target radionuclide concentration determinations is the fact that signals required for such determinations are either too weak or nonexistent in the calibration data. Of the radionuclides that occur in waste at the Hanford Site, only two exist in the calibration standards:  $^{235}\text{U}$  and  $^{238}\text{U}$ . The associated gamma rays (185.7 keV and 1001.0 keV, respectively) have such low yields that the calibration standards do not have uranium concentrations high enough to produce adequate signals for calibrations.

Koizumi (2001) noted that the only gamma-ray sources in the calibration standards are potassium, uranium, and thorium, but this means that the calibration measurements provide data that can be used to calculate the natural potassium, uranium, and thorium backgrounds in spectral windows. Koizumi presented equations for such calculations. The equations could be used to calculate the potassium, uranium, and thorium backgrounds in a window, then the total background could be subtracted from the recorded window count rate to isolate the window count rate due to a target radionuclide. With a spectrum from a  $^{137}\text{Cs}$ -contaminated zone, for example, the background count rate in the  $^{137}\text{Cs}$  window could be determined and subtracted from the total window count rate to estimate the count rate due only to  $^{137}\text{Cs}$ . That  $^{137}\text{Cs}$  count rate could then be correlated to the  $^{137}\text{Cs}$  concentration established from an SGLS log. A relationship between background-free window count rates and  $^{137}\text{Cs}$  concentrations could be deduced from a number of such correlations. This relationship would be a  $^{137}\text{Cs}$  calibration, but it would be primitive at best, for several reasons. Propagation of uncertainties through the calculations would impose extremely large relative uncertainties on any calculated  $^{137}\text{Cs}$  concentrations. The energies of the gamma rays from the target radionuclide would have to be less than about 1390 keV because gamma rays with energies exceeding 1390 keV would add counts to the potassium, uranium, or thorium windows, and incorrect background values would result. Furthermore, if more than one target radionuclide was present, there would be additional

background window counts that would be difficult or impossible to determine. The method has not been implemented because of these limitations, and also because the current data analysis deals primarily with total counts instead of window counts. If a desire to test the method should arise, the data required for development of background subtraction are tabulated in Tables 4-2, 4-3, and 4-4.

## 5.0 Revised Field Verification Acceptance Criteria

During logging operations, spectra are recorded before and after each logging run with a field verification gamma-ray source mounted on the RAS sonde. Total counts and selected window counts are calculated and compared to acceptance criteria to confirm the proper operation of the data acquisition system.

The field verification source was procured from AEA Technology specifically for RAS measurements. The source product name is *KUTh Field Verifier* and the product code number is 188701. The source contains  $^{40}\text{K}$ ,  $^{238}\text{U}$ , and its decay progenies (the source contains  $^{235}\text{U}$  also, but the contribution to a gamma-ray spectrum by this nuclide is negligible), and  $^{232}\text{Th}$  and its decay progenies. The decay activities (as determined on December 12, 2000) are displayed in Table 5-1.

Table 5-1. Sources in the KUTh Field Verifier

Source	Activity (microcuries)	Half Life (years)
$^{40}\text{K}$	1.663	$1.3 \times 10^9$
$^{238}\text{U}$	0.46	$4.5 \times 10^9$
$^{232}\text{Th}$	0.331	$1.4 \times 10^{10}$

The long half lives of these sources ensure that the decay activities are essentially constant over time. It is assumed that the decay progenies of  $^{238}\text{U}$  and  $^{232}\text{Th}$  are present in quantities consistent with decay equilibrium. Thus, there is no expectation of any increase in gamma-ray output associated with a buildup of gamma-ray-emitting decay products such as  $^{214}\text{Bi}$  (decay product of  $^{238}\text{U}$ ) and  $^{208}\text{Tl}$  (decay product of  $^{232}\text{Th}$ ).

RAS field verification acceptance criteria were originally formulated in terms of warning limits and control limits. If a number of field verification spectra yielded a set of counts or count rates for a particular window with a mean  $\langle R \rangle$  and a standard deviation  $\sigma R$ , the warning limits for a new measurement were  $\langle R \rangle - 2\sigma R$  and  $\langle R \rangle + 2\sigma R$ , and the control limits were  $\langle R \rangle - 3\sigma R$  and  $\langle R \rangle + 3\sigma R$ . The logging system passed a verification test if a new reading yielded an  $R$  value between the warning limits. If the new reading lay outside of the warning limits or outside of the control limits, the system was checked for evidence of malfunction.

Recently, the field verification acceptance test was modified. The use of warning limits was discontinued; window and total count rates are now compared only to control limits. Count rate control limits are specified for the  $^{40}\text{K}$  window (1390 to 1600 keV), the  $^{238}\text{U}$  window (1600 to 2400 keV), and the total spectrum count rate. The  $^{40}\text{K}$  window is narrow and the count rate will be sensitive to the position of the 1460.8-keV gamma-ray peak within the window. The window count rate should therefore provide a measure of the system gain stability. The  $^{238}\text{U}$  window is wider, and the count rate should be somewhat dependent on the system gain and efficiency. The total spectrum count rate is expected to be relatively insensitive to gain shift, but sensitive to changes in system efficiency.

Control limits were derived from the count rate data in Tables 5-2, 5-4, and 5-6. The control limits are displayed in Table 5-3 (large detector), Table 5-5 (medium detector), and Table 5-7 (small detector).

Table 5-2. Large Detector Field Verification Data

<b>Spectrum File Name</b>	<b>Live Time (seconds)</b>	<b>Percent Dead Time</b>	<b>Potassium Window Count Rate (counts per second)</b>	<b>Uranium Window Count Rate (counts per second)</b>	<b>Total Count Rate (counts per second)</b>
LVUB1000.CHN	200	0.053	182.14	192.97	6005.1
LVUB1001.CHN	200	0.053	185.06	192.34	5999.0
LVUB1002.CHN	200	0.053	185.30	194.49	6008.1
LVUB1003.CHN	200	0.053	185.00	197.91	6011.0
LVUB1004.CHN	200	0.053	183.52	200.68	6005.9
LVUB1005.CHN	200	0.053	183.87	201.95	6020.0
LVUBK001.CHN	200	0.054	185.01	193.33	6144.8
LVUBK002.CHN	200	0.054	183.61	190.92	6124.5
LVUBK003.CHN	200	0.054	183.31	190.52	6122.1
LVUBK004.CHN	200	0.054	181.57	191.51	6126.6
LVUBK005.CHN	200	0.054	183.86	190.56	6121.6
LVUBK006.CHN	200	0.054	181.09	190.37	6126.8

Table 5-3. Large Detector Control Limits

<b>Window</b>	<b>Lower Control Limit (counts per second)</b>	<b>Upper Control Limit (counts per second)</b>
Potassium	179.4	187.8
Uranium	181.8	206.1
Total	5879	6257

Table 5-4. Medium Detector Field Verification Data

<b>Spectrum File Name</b>	<b>Live Time (seconds)</b>	<b>Percent Dead Time</b>	<b>Potassium Window Count Rate (counts per second)</b>	<b>Uranium Window Count Rate (counts per second)</b>	<b>Total Count Rate (counts per second)</b>
MVUB2000.CHN	600	0.004	6.64	7.99	550.27
MVUB2001.CHN	600	0.004	6.71	7.78	552.00
MVUB2002.CHN	600	0.004	6.69	7.86	551.71
MVUB2003.CHN	600	0.004	6.76	7.80	551.51
MVUB2004.CHN	600	0.004	6.64	8.08	553.65
MVUB2005.CHN	600	0.004	6.82	7.90	553.51
MVUBR000.CHN	600	0.004	6.90	8.09	553.86
MVUBR001.CHN	600	0.004	6.83	8.12	554.77
MVUBR002.CHN	600	0.005	6.71	8.33	556.22
MVUBR003.CHN	600	0.005	6.72	8.15	556.57
MVUBR004.CHN	600	0.005	6.71	8.39	558.26
MVUBR005.CHN	600	0.005	6.98	8.26	559.94

Table 5-5. Medium Detector Control Limits

<b>Window</b>	<b>Lower Control Limit (counts per second)</b>	<b>Upper Control Limit (counts per second)</b>
Potassium	6.44	7.08
Uranium	7.45	8.67
Total	545.6	563.1

Table 5-6. Small Detector Field Verification Data

<b>Spectrum File Name</b>	<b>Live Time (seconds)</b>	<b>Percent Dead Time</b>	<b>Potassium Window Count Rate (counts per second)</b>	<b>Uranium Window Count Rate (counts per second)</b>	<b>Total Count Rate (counts per second)</b>
SVUB3000.CHN	1000	0.001	1.134	1.55	130.2
SVUB3001.CHN	1000	0.001	1.149	1.52	130.7
SVUB3002.CHN	1000	0.001	1.197	1.44	130.9
SVUB3003.CHN	1000	0.001	1.144	1.55	130.6
SVUB3004.CHN	1000	0.001	1.204	1.51	131.1
SVUB3005.CHN	1000	0.001	1.197	1.45	131.1
SVUBN000.CHN	1000	0.001	1.165	1.48	132.2
SVUBN001.CHN	1000	0.001	1.160	1.55	132.4
SVUBN002.CHN	1000	0.001	1.165	1.54	132.3
SVUBN003.CHN	1000	0.001	1.163	1.52	133.2
SVUBN004.CHN	1000	0.001	1.150	1.54	132.3
SVUBN005.CHN	1000	0.001	1.238	1.60	132.4

Table 5-7. Small Detector Control Limits

<b>Window</b>	<b>Lower Control Limit (counts per second)</b>	<b>Upper Control Limit (counts per second)</b>
Potassium	1.081	1.263
Uranium	1.39	1.65
Total	128.7	134.5

A field verification test is conducted as follows. A field verification spectrum is recorded, the  $^{40}\text{K}$  window,  $^{238}\text{U}$  window, and total spectrum count rates are calculated, and the count rates are compared with the appropriate control limits. If a count rate falls outside of the control limit range, the system fails the field verification test. Failures are reported to the Hanford Office Technical Lead, and the cause of any failure is determined and corrected before additional logging is performed.

## List of References

- Friedlander, G., J.W. Kennedy, E.S. Macias, and J.M. Miller, 1981. *Nuclear and Radiochemistry*, John Wiley and Sons, New York.
- Heistand, B.E., and E.F. Novak, 1984. *Parameter Assignments for Spectral Gamma-Ray Borehole Calibration Models*, GJBX-2(84), prepared by Bendix Field Engineering Corporation for the U.S. Department of Energy Grand Junction Projects Office, Grand Junction, Colorado.
- Koizumi, C.J., 2001. *Hanford Tank Farms Vadose Zone Monitoring Project Initial Calibration of the Radionuclide Assessment System*, GJO-2001-237-TAR, prepared by MACTEC-ERS for the U.S. Department of Energy Grand Junction Office, Grand Junction, Colorado.
- Steele, W.D., and D.C. George, 1986. *Field Calibration Facilities for Environmental Measurement of Radium, Thorium, and Potassium*, GJ/TMC-01 (Second Edition) UC-70A, prepared by Bendix Field Engineering Corp. for the U.S. Department of Energy Grand Junction Projects Office, Grand Junction, Colorado.
- Stromswold, D.C., 1978. *Monitoring of the Airport Calibration Pads at Walker Field, Grand Junction, Colorado for Long-Term Radiation Variations*, GJBX-99(78), prepared by Bendix Field Engineering Corporation for the U.S. Department of Energy Grand Junction Projects Office, Grand Junction, Colorado.
- Trahey, N.M., A.M. Voeks, and M.D. Soriano, 1982. *Grand Junction/New Brunswick Laboratory Interlaboratory Measurement Program, Part I: Evaluation, Part II: Methods Manual*, Report NBL-303, New Brunswick Laboratory, Argonne, Illinois.
- Wilson, R.D., and D.C. Stromswold, 1981. *Spectral Gamma-Ray Logging Studies*, GJBX-21(81), prepared by Bendix Field Engineering Corporation for the U.S. Department of Energy Grand Junction Projects Office, Grand Junction, Colorado.

**Appendix A**  
**Gamma-Ray Calibration Standards**

## Appendix A Gamma-Ray Calibration Standards

### A.1 Calibration Standards

Calibration standards for borehole gamma-ray sensors are located at a Hanford Site calibration center, which is near the Meteorology Station, north of the main entrance to the 200 West Area. Steele and George (1986) and Heistand and Novak (1984) describe these calibration standards and their links to certified radiation counting standards.

Steele and George refer to four calibration models named the “Spokane SBL/SBH, SBT/SBK, SBU/SBM, and SBA/SBB Models” (Steele and George 1986, page B-24). Each model is a stack of five right circular concrete cylinders enclosed in a cylindrical steel tank. In sequence from the bottom, the cylinders are a 2-ft-thick barren cylinder, a 4-ft-thick lower calibration standard, a 5-ft-thick middle barren cylinder, a 4-ft-thick upper calibration standard, and a 2.5-ft-thick upper barren cylinder. Each model has two calibration standards separated by a thick middle barren cylinder that shields measurements in one standard from the radiation from the other standard.

Barren cylinders are made of ordinary concrete with background concentrations of the natural radionuclides: potassium-40 ( $^{40}\text{K}$ ), uranium-235 ( $^{235}\text{U}$ ) and its decay products, uranium-238 ( $^{238}\text{U}$ ) and its decay products, and thorium-232 ( $^{232}\text{Th}$ ) and its decay products.

The name of each model incorporates the names of the two calibration standards in the model. For example, the standards in model SBL/SBH are named SBL and SBH. The letters in the names of the standards have the meanings indicated by the entries in Table A-1.

Table A-1. Key to Calibration Standard Names

Letter	Meaning	Notes
S	Spokane	This is a reference to the original installation of these models by DOE Grand Junction Site in the early 1980s at a calibration facility near Spokane, Washington.
B	Borehole	This distinguishes the standards for borehole sensors from other standards at Spokane that were designed for calibration of hand-held surface scanning instruments.
K U T	Potassium Uranium Thorium	SBK has an elevated concentration of potassium. Likewise, SBU and SBT have elevated uranium and thorium concentrations, respectively.
M	Mixed	The SBM standard has elevated concentrations of potassium, uranium, and thorium.
L H	Low High	SBL and SBH are low and high uranium standards that were designed for calibration of gross gamma-ray logging systems.
A B	(none)	SBA and SBB are low and high uranium standards that were designed for the calibration of fission neutron logging systems.

Each model has 4.5-inch-diameter test hole that coincides with the model cylinder axis and penetrates all of the zones. The dimensions of the standards are large enough to simulate

“infinite media,” meaning that the gamma-ray flux within the test hole at the center of any standard is indistinguishable from the flux that would exist if the medium had the same concentrations of gamma-ray sources, but were infinite in extent.

The calibration standards contain orthoclase feldspar, uraninite and other uranium minerals, and monazite. These minerals contain the gamma-ray sources  $^{40}\text{K}$ ,  $^{238}\text{U}$ , and other members of the uranium decay chain, including radium-226 ( $^{226}\text{Ra}$ ), and  $^{232}\text{Th}$  and other members of the thorium decay chain. The concentrations of the gamma-ray sources are displayed in Table A-2 (from Steele and George 1986).

Table A-2. Calibration Standard Source Concentrations

Standard	$^{40}\text{K}$ Concentration (pCi/g)	$^{226}\text{Ra}$ Concentration (pCi/g)	$^{232}\text{Th}$ Concentration (pCi/g)
SBK	53.50 ± 1.67	1.16 ± 0.11	0.11 ± 0.02
SBU	10.72 ± 0.84	190.52 ± 5.81	0.66 ± 0.06
SBT	10.63 ± 1.34	10.02 ± 0.48	58.11 ± 1.44
SBM	41.78 ± 1.84	125.79 ± 4.00	39.12 ± 1.07
SBA	undetermined	61.2 ± 1.7	undetermined
SBL	undetermined	324 ± 9	undetermined
SBB	undetermined	902 ± 27	undetermined
SBH	undetermined	3126 ± 180	undetermined

The concentrations in Table A-2 are referenced to the gamma-ray counting standards in Table A-3. The 100-A standards are certified by the New Brunswick Laboratory (Trahey et al. 1982).

Table A-3. Reference Standards for Calibration Standard Source Concentrations

Source	Reference Standard
Potassium ( $^{40}\text{K}$ )	reagent-grade potassium carbonate ( $\text{K}_2\text{CO}_3$ )
Radium ( $^{226}\text{Ra}$ )	NBL (New Brunswick Laboratory) 100-A Series Uranium
Thorium ( $^{232}\text{Th}$ )	NBL 100-A Series Thorium <sup>1</sup>

The concentrations in Table A-2, and all concentrations quoted in this report, are actually decay rates per unit mass expressed in picocuries per gram (pCi/g). A picocurie is  $10^{-12}$  of a curie, and a curie is  $3.7 \times 10^{10}$  disintegrations per second, by definition. Decay rates per unit mass are customarily cited in environmental radiation surveys, where the decay activity usually has more significance than the mass of radionuclide per unit sample mass.

## A.2 Gamma-Ray Sources

### A.2.1 Potassium

Natural potassium consists mostly of two nonradioactive isotopes, potassium-39 (about 93.3 percent) and potassium-41 (about 6.7 percent). Approximately 0.01 percent of natural potassium is  $^{40}\text{K}$ .  $^{40}\text{K}$  has such a long half life (1.3 billion years) that the decay rates in the calibration standards are essentially constant over time.  $^{40}\text{K}$  has two decay modes: beta decay (branching ratio = 0.893) yields calcium-40, and electron capture (branching ratio = 0.107) yields argon-40 in an excited state. The argon-40 transition to the ground state is accompanied by emission of the well known 1460.8-keV “potassium gamma ray.” Calcium-40 and argon-40 are stable.

### A.2.2 Uranium

The uranium isotopes present in natural uranium in significant quantities are  $^{238}\text{U}$  (about 99.3 percent) and  $^{235}\text{U}$  (about 0.7 percent). Natural uranium contains a third isotope,  $^{234}\text{U}$ , at a level of about 0.0055 percent.  $^{234}\text{U}$  is the third decay product of  $^{238}\text{U}$ . The half life of  $^{234}\text{U}$  is a small fraction of the age of the earth, so  $^{234}\text{U}$  would not exist in nature if it were not constantly replenished by the decay of the more long lived  $^{238}\text{U}$ .

$^{235}\text{U}$  is the first nuclide in a decay chain known as the actinium series. The last nuclide in the actinium series is the stable lead isotope lead-207. As gamma-ray sources, the members of the actinium series are of minor importance compared to the decay products of  $^{238}\text{U}$ . The sources and energies for the three most intense actinium series gamma rays are  $^{235}\text{U}$ , 185.7 keV; radium-223, 269.5 keV; and bismuth-211, 351.1 keV. For natural uranium, these gamma rays have weak intensities and their signals are noteworthy only as minor interferences to more prominent spectral peaks in high resolution spectrometry. For example, the 351.1-keV gamma ray adds a minute contribution to the spectral peak for the 351.9-keV gamma ray of lead-214 ( $^{214}\text{Pb}$ ), which is a decay product of  $^{238}\text{U}$ .

The uranium series is the decay chain that starts with  $^{238}\text{U}$  and ends with the stable lead isotope lead-206. The half life of  $^{238}\text{U}$ , approximately 4.5 billion years, is far greater than the half life of any other radionuclide in the uranium series. For an isolated sample containing a long-lived radionuclide that decays to short-lived progenies, the radioactive decay equations predict (Friedlander et al., 1981) that as time passes the decay rate of each progeny will approach the decay rate of the long-lived radionuclide at the top of the decay chain. Thus, if a sample containing  $^{238}\text{U}$  ages for a sufficient time without exchanging material with the environment outside of the sample, all of the radioactive  $^{238}\text{U}$  decay progenies will attain the same decay rate, which will be identical to the decay rate of  $^{238}\text{U}$ . In this situation, each decay product is said to be in “secular equilibrium” with  $^{238}\text{U}$ .

Between  $^{238}\text{U}$  and lead-206 are seventeen radioactive decay products. Four of these, astatine-218, thallium-210, mercury-206, and thallium-206, lie on decay paths with very small branching ratio values and are inconsequential to gamma-ray spectrometry.

Radium-226 ( $^{226}\text{Ra}$ ), the fifth decay product of  $^{238}\text{U}$ , is critically important to gamma-ray

spectrometry. The most prolific gamma-ray sources in the uranium series,  $^{214}\text{Pb}$  and bismuth-214 ( $^{214}\text{Bi}$ ), both occur below  $^{226}\text{Ra}$  in the  $^{238}\text{U}$  decay chain, but  $^{226}\text{Ra}$  has a moderately long half life (1,600 years) and is chemically dissimilar to uranium. Geochemical processes can upset decay equilibrium in a uranium deposit by preferentially altering the uranium or radium concentration. If this occurs, the  $^{226}\text{Ra}$  and  $^{238}\text{U}$  decay rates in a sample from the deposit will obviously be unequal, and analyses based on the  $^{214}\text{Pb}$  and  $^{214}\text{Bi}$  gamma rays will produce erroneous uranium concentration values. However, the radioactive decay progenies of  $^{226}\text{Ra}$ , including  $^{214}\text{Pb}$  and  $^{214}\text{Bi}$ , have half lives that are much shorter than the half life of  $^{226}\text{Ra}$ , so the  $^{226}\text{Ra}$  decay products are generally in secular equilibrium with  $^{226}\text{Ra}$ .

It is possible for the  $^{226}\text{Ra}$  decay products in a uranium-radium sample to be out of equilibrium with  $^{226}\text{Ra}$  if the sample is porous.  $^{226}\text{Ra}$  decays to radon-222 ( $^{222}\text{Rn}$ ),  $^{222}\text{Rn}$  decays to polonium-218, and polonium-218 decays to  $^{214}\text{Pb}$ , which decays to  $^{214}\text{Bi}$ .  $^{222}\text{Rn}$  is a noble gas with a 3.8-day half life. If  $^{222}\text{Rn}$  escapes from a sample, the concentrations of polonium-218,  $^{214}\text{Pb}$ , and  $^{214}\text{Bi}$  will obviously be smaller than the concentrations that would exist under decay equilibrium.

The gamma-ray source intensities for SBU, SBM, SBA, SBL, SBB, and SBH were established via gamma-ray spectrometry, and Steele and George (1986) present the source intensities in terms of  $^{226}\text{Ra}$  concentrations instead of  $^{238}\text{U}$  concentrations. This acknowledges that the  $^{214}\text{Pb}$  and  $^{214}\text{Bi}$  gamma-ray signals utilized by the spectral measurements could be correlated to  $^{226}\text{Ra}$  concentrations, but  $^{226}\text{Ra}$  and  $^{238}\text{U}$  might be out of equilibrium. However, the uranium in the calibration standards is in minerals that are presumably millions of years old, so the  $^{226}\text{Ra}$  in any standard is likely to be in secular equilibrium with the  $^{238}\text{U}$  in the standard.

Studies by Stromswold (1978) and others indicated that  $^{222}\text{Rn}$  does not escape from water-saturated media. The calibration standards are therefore maintained in a saturated condition to prevent  $^{222}\text{Rn}$  leakage. Moisture in unconsolidated vadose zone sediments cannot be similarly controlled, so  $^{222}\text{Rn}$  concentrations in such unsaturated, porous media can be influenced by changes in atmospheric pressure. Atmospheric pressure changes most likely account for temporal variations in the apparent concentrations of natural uranium that are occasionally inferred from monitoring logs from vadose zone boreholes.

### A.2.3 Thorium

Essentially 100 percent of natural thorium is  $^{232}\text{Th}$ .  $^{232}\text{Th}$  and its decay products are members of the decay chain known as the thorium series. The last nuclide in the thorium series is the stable lead isotope lead-208. Like  $^{238}\text{U}$ ,  $^{232}\text{Th}$  has a half life ( $T_{1/2} = 14$  billion years) that far exceeds the half lives of any of its radioactive decay products. The longest-lived radioactive progenies of  $^{232}\text{Th}$  are radium-228 ( $T_{1/2} = 6.7$  years) and thorium-228 ( $T_{1/2} = 1.9$  years). Thallium-208 ( $^{208}\text{Tl}$ ), a significant gamma-ray source in the thorium series, is analogous to  $^{214}\text{Pb}$  and  $^{214}\text{Bi}$  in the uranium series; the half life of  $^{208}\text{Tl}$  is short ( $T_{1/2} = 3.1$  minutes) and the nuclide lies near the end of the decay chain. The half lives of the  $^{232}\text{Th}$  decay products are all so short that secular equilibrium is the norm and thorium assays based on the  $^{208}\text{Tl}$  gamma rays are almost always accurate. The thorium series has a noble gas, radon-220 ( $^{220}\text{Rn}$ ), that precedes  $^{208}\text{Tl}$  in the decay chain, but leakage of  $^{220}\text{Rn}$  from a thorium sample seldom causes a measurable departure from secular equilibrium because the half life of  $^{220}\text{Rn}$  is only 55 seconds. If a thorium sample were to

lose all of its  $^{220}\text{Rn}$ , but then experience no further losses, the concentration of  $^{220}\text{Rn}$  would grow to 99.5 percent of the equilibrium value in about eight minutes.